# Lessons Learned from Dike Failures in Recent Decades

**Cor Zwanenburg**, *Deltares, Delft, The Netherlands, email: cor.zwanenburg@deltares.nl*
**Norma Patricia López-Acosta**, *UNAM, Mexico City, Mexico*
**Rémy Tourment**, *Irstea, Marseille, France*
**Alessandro Tarantino,** *University of Strathclyde, Glasgow, United Kingdom*
**Annarita Pozzato,** *University of Strathclyde, Glasgow, United Kingdom*
**Alexandre Pinto**, *JetSJ, Lisbon, Portugal*

**ABSTRACT**: *The paper describes five different dike failures that occurred in recent decades. The case histories were located on different rivers and involved different loading conditions. The observed failure mechanisms involved erosion and stability problems. The types of erosion observed were both internal erosion due to extreme groundwater flow and external erosion caused by the river flow and wave action. The case involving instability was caused by uplift, i.e., increased hydraulic head led to a sharp reduction in maximum shear strength between subsoil layers. Two cases demonstrate the importance of dike management and maintenance. Despite the variations in the loading conditions and failure mechanisms, all the cases show that the strength of a dike depends not only on the material used to build the dike but also on the strength of the subsoil.*

**KEYWORDS:** dikes, failure, erosion, stability, uplift

**LOCATIONS**: Geo-Database

## INTRODUCTION

The data presented in the World Disasters Report (IFRCRCS, 2016) show that flooding is one of the most dangerous natural hazards faced by mankind. With 1751 reported events between 2006 and 2015, 45% of all reported natural disasters were floods. During this period, flooding accounted for 8% of human fatalities involving natural disasters, 24.5% of the financial costs, and 44% of the people affected. These numbers emphasize the importance of flood risk management. Given the increasing world population and the expectation of sea-level rise owing to climate change, flood risk management will become increasingly important.

Dike construction and maintenance play a crucial role in flood risk management systems. Technical Committee 201, "Dikes and Levees", of the International Society for Soil Mechanics and Geotechnical Engineering (ISSMGE TC201) focuses on improving the understanding of how dikes behave. Five cases of recent dike failures were selected from the extensive experience available in the committee. The cases are discussed in the present paper and demonstrate the complexity of dike behaviour, as the dike and the subsoil are required to jointly withstand water loads in design conditions.

## CASE HISTORY #1: VILLAHERMOSA, TABASCO, MEXICO

### Background

The Grijalva basin in Tabasco State, Mexico, consists of a complex system of rivers that converge mostly in two rivers that pass through the city of Villahermosa: the Carrizal and the Grijalva (Figure 1). In order to protect this city and other towns in the state from flooding, two types of dikes have been built: (a) dikes built on the banks of the rivers (Figure 2a), and (b) dikes built around exposed urban areas (Figure 2b). Flooding in the Grijalva watershed in 2007 demonstrated the vulnerability of these structures. In many instances, the problems were found to be geotechnical: they were largely attributed to rapid filling and drawdown conditions caused by fluctuations in river, lagoon or reservoir levels and to the seepage forces – the hydraulic

Submitted: 29 December 2016; Published: 28 June 2018
Reference: Zwanenburg, C., López-Acosta, N.P., Tourment, R., Tarantino, A., Pozzato, A. and Pinto, A. (2018). *Lessons Learned from Dike Failures in Recent Decades*. International Journal of Geoengineering Case histories, Vol.4, Issue 3, p.203-229. doi: 10.4417/IJGCH-04-03-04

gradients generated by these fluctuations – and rain infiltration in the crests of the dikes (Figure 3). Auvinet et al. (2008) observed that problems in river banks commonly begin with erosion which, depending on the type of soil, can cause piping in some areas, possibly resulting in landslides (Figure 4). These eroded sections are generally protected with dikes consisting of clayey material. Elements that can better withstand erosion by river water are also used, examples being rock fill, systems with concrete bags (*bolsacreto* or *colchacreto*), breakwaters or sheet pile walls. River embankments may also fail when the weight of these structures exceeds the bearing capacity of the foundation soil (Figure 3). Generally, failure occurs in layers with low shear strength such as the highly compressible clays and peats which are found in unpredictable locations along the banks of the rivers in Villahermosa (Figure 1). It has also been found that factors such as scour of the riverbed and over-loading caused by the weight of additional protection such as sand bags result in dike instability. In addition, intense rainfall in the region can cause large and rapid variations in the levels of local rivers, lagoons and reservoirs.

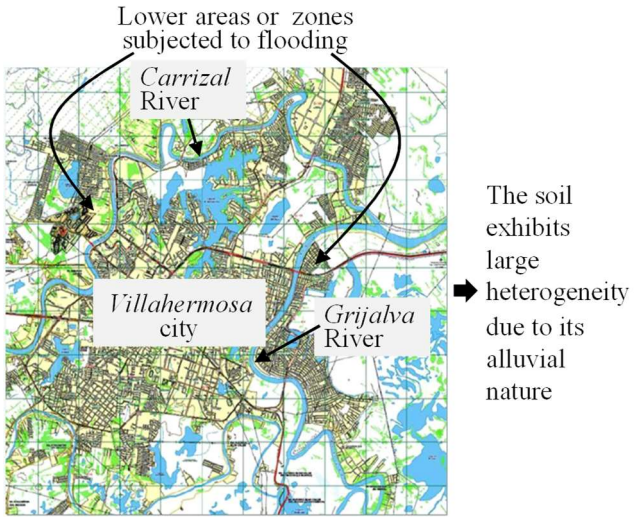


*Figure 1. Rivers passing through the city of Villahermosa (Tabasco State, Mexico)*

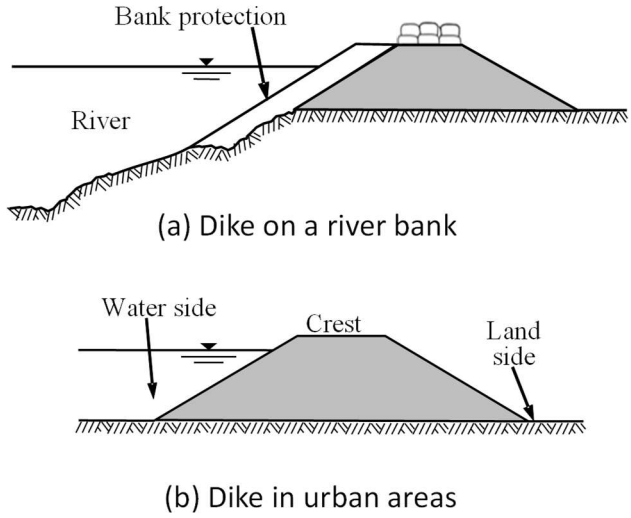


*Figure 2. Types of dikes in Villahermosa, Mexico*

*Figure 3. Consequences of water drawdown in Tabasco State, Mexico*

**Rapid Drawdown**

Sudden or rapid drawdown occurs when there is an unexpected drop in the outside water level that modifies the flow conditions in the structure without adequate time for drainage of the soil mass. Hydraulic gradients and seepage forces develop that, in extreme conditions, cause soil erosion problems that range from minor to severe, examples being piping or even the complete failure of the structure. In addition, rapid drawdown has a negative effect on slope stability and it may result in the

failure of the slope. Rapid drawdown is a complex problem that is influenced by variations in the magnitude and rate of drawdown, hydraulic conductivity, the porosity of materials, the geometry of the slope and the initial boundary conditions of the flow.


*Figure 4. Evidence of instability in river banks and dikes induced by rapid drawdown in Villahermosa.*

**Simplified Parametric Analyses: Application to the Study of Dikes**

Transient flow analyses to assess how water drawdown affects soil erosion in dikes built to provide protection from flooding in regions affected by intense rainfall are made using numerical modelling. Modelling is based on the finite element method (FEM) with the SEEP/W code (GEO-SLOPE Int. Ltd., 2008) and the mathematical model of Van Genuchten (1980) for unsaturated flow. More detail can be found in López-Acosta et al. (2015). The simplified geometry and general boundary conditions for the analysed domain can be found in Figure 5. A water level on the riverside of the dike body is assumed (high water level = 11.5 m) that drops rapidly to a lower water level of 6.0 m. The total water drawdown is 5.5 m. A steady-state condition is initially assumed in the dike. The dike material is considered to be homogeneous and isotropic to better appreciate its behaviour in response to different rates of drawdown $R_d$ and for a range of soils with distinct saturated hydraulic conductivities $k_s$ as well as variations in the slope ratios of the dike body. These three variables were assessed in several parametric analyses that were conducted by varying one of the variables of interest on each occasion and assuming that the other variables were constant. Each analysis was stopped at the end of the drawdown stage. The analyses assumed a continuous time-dependent variation in the water level under transient-state flow conditions. Table 1 provides a description of the material and both the residual and saturated volumetric water contents associated with saturated hydraulic conductivities $k_s$ assumed in this study. These water contents were used to assess, using the Van Genuchten model, the corresponding unsaturated soil property functions considered in the present study (Figure 6).

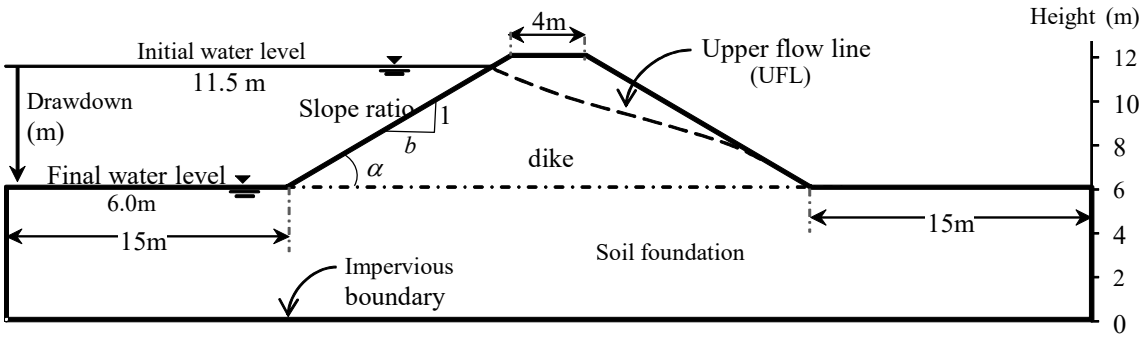


*Figure 5. Simplified geometry, initial hydraulic and boundary conditions in the dike studied (López-Acosta et al. 2015).*

*Table 1. Materials and hydraulic properties assumed for predicting unsaturated soil property functions using the Van Genuchten model*

| $k_s$ (m/s) | Soil Type | $\theta_s$ | $\theta_r$ | Fitting parameters | | |
|---|---|---|---|---|---|---|
| | | | | *a* | *N* | *m* |
| $1\times10^{-04}$ | Silty sand | 0.32 | 0.02 | 1 | 4.2 | 0.76 |
| $1\times10^{-05}$ | Sandy silt | 0.37 | 0.018 | 7 | 2.93 | 0.58 |
| $1\times10^{-06}$ | Clayey silt | 0.40 | 0.014 | 15 | 1.80 | 0.44 |
| $1\times10^{-07}$ | Silty clay | 0.45 | 0.010 | 32 | 1.56 | 0.38 |
| $1\times10^{-08}$ | Clay | 0.50 | 0.010 | 55 | 1.47 | 0.32 |

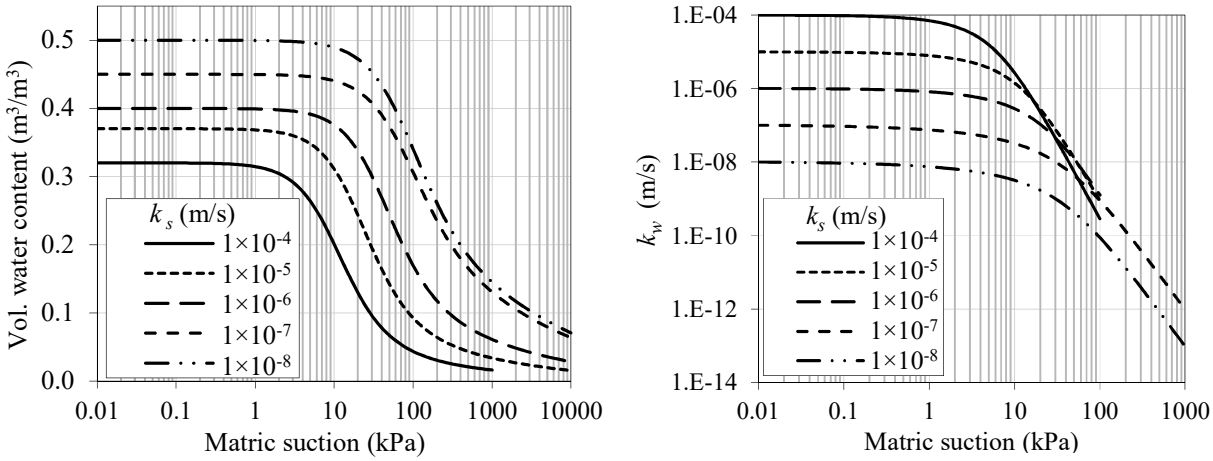


(a) Storage functions estimated with Van Genuchten model

(b) Conductivity functions estimated with Van Genuchten model

*Figure 6. Unsaturated soil property functions assumed in analyses (López-Acosta et al. 2015)*

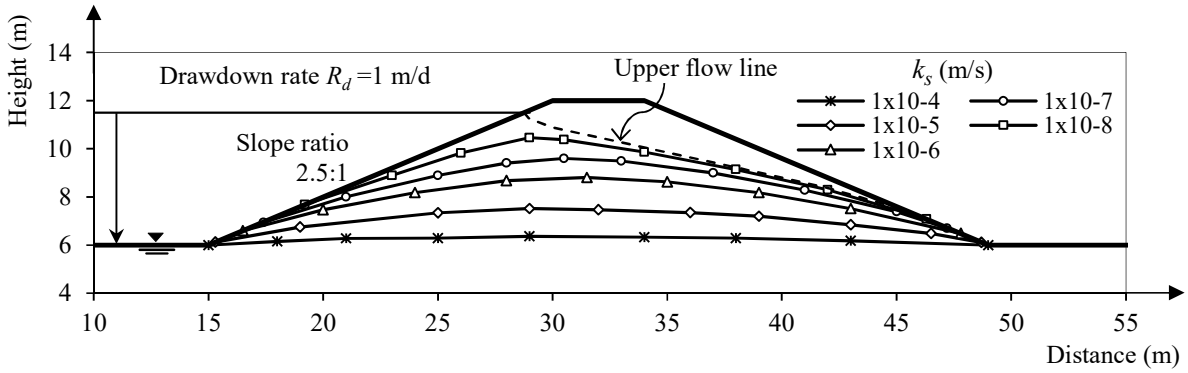


*Figure 7. Phreatic surfaces (desaturation lines) at the end of the water drawdown stage in a dike with variable hydraulic conductivities $k_s$, (López-Acosta et al. 2015)*

These analyses evaluated several homogeneous and isotropic dikes with a 2.5(H):1(V) slope and total dewatering head of 5.5 m for different hydraulic conductivities. Figure 7 shows the upper flow line for the initial steady-state condition and desaturation lines at the end of water drawdown in dikes with different hydraulic conductivities $k_s$ for the transient-state condition and assuming a constant drawdown rate of $R_d$ = 1 m/d. As can be seen from this figure, where $k_s = 1\times10^{-08}$ m/s, the desaturation line remains practically in the same position as the upper flow line, which is associated with the *fully rapid drawdown mode*. In this case, it can be assumed that the soil behaves undrained. For $k_s = 1\times10^{-04}$ m/s, the desaturation line inside the dike drops down almost in line with the reservoir water level, which is associated with the *fully slow drawdown mode*. In this case, it can be assumed that the soil behaves drained. It can also be assumed that the desaturation lines between these two extreme modes represent the *transient drawdown mode* in which a curvilinear water line is generated in the soil structure, the position of which depends on the drawdown rate and the constitutive material properties. The remaining pore pressure in the dike is therefore transient, it varies as a function of time, but also with the soil's ability to retain water. Several authors have recognised the three water drawdown modes described here (examples being Lane & Griffiths, 2000 and Berilgen, 2007).

Figure 8 shows the effect of the drawdown rate on exit hydraulic gradients in the horizontal and vertical directions, corresponding to the x and y axes respectively, in both the upstream and downstream slopes of the dikes with variable hydraulic conductivities $k_s$. In addition, Figure 9 summarizes the results obtained assuming variable permeabilities $k_s$ and a constant drawdown rate ($R_d$ = 1 m/d). The following conclusions can be drawn on the basis of the results of these parametric analyses:

- Under a steady-state flow, the exit hydraulic gradients in the downstream slope remain constant for all $k_s$ permeabilities studied.
- Changes in the slope ratio of dikes have a more significant effect on the magnitude of the exit hydraulic gradients than changes in the drawdown rate. It was observed that steeper slopes generate greater values for exit gradients.
- The hydraulic gradients are more sensitive to variations in the slope ratio in dikes consisting of materials with medium to low permeability than in dikes with permeable materials, where the hydraulic gradients remain approximately the same even when the slope ratio changes.
- The more impermeable a material is, the larger the exit hydraulic gradients. In this sense, the maximum value of the exit gradient in the upstream slope tends to match the value of the computed gradient in the downstream slope under steady-state conditions.
- The exit hydraulic gradients were observed to increase when the drawdown rate increased.
- In general, given the admissible values suggested by several authors for local erosion and piping (for example, Den Adel et al., 1988; Wan & Fell, 2004; Ahlinhan & Achmus, 2010), the magnitude of the gradients computed here is significant. One suitable way of preventing internal erosion or piping is the installation of filters or drains placed strategically in the earth structure.

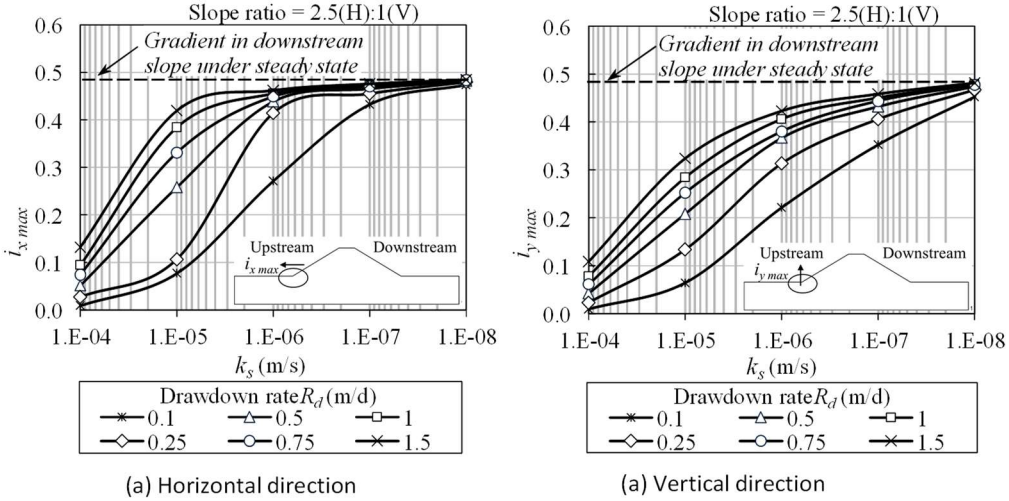


*Figure 8. Effect of drawdown rate $R_d$ on exit hydraulic gradients in dikes for variable hydraulic conductivities $k_s$, (López-Acosta et al. 2015)*

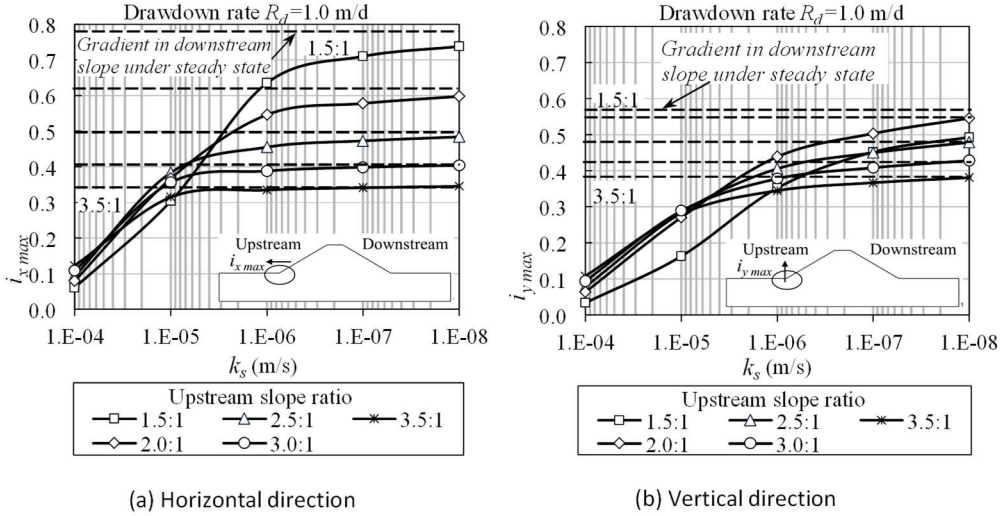


*Figure 9. Effect of the slope ratio (H:V) on exit hydraulic gradients in dikes for different hydraulic conductivities $k_s$, (López-Acosta et al. 2015)*

**General Concluding Remarks**

This study focused on one of the main problems affecting the stability of Tabasco dikes: the water drawdown phenomenon caused by sudden changes in the levels of rivers, lagoons and reservoirs. Particular emphasis was placed on the study of exit hydraulic gradients at the toe of homogeneous and isotropic dikes. The effects of different parameters (drawdown rate, hydraulic conductivity and slope ratio) for the dikes were assessed in unsaturated, transient-state, flow analyses based on numerical modelling with the finite element method. Based on the results, it is concluded that analyses should consider the susceptibility to erosion of the material used to build the dike. However, analyses should also include measures – such as the installation of drains and filters – to reduce the hydraulic gradients and seepage forces generated inside the soil mass. The results of the analysis led to the practical recommendations shown in Figure 10, which should be taken into consideration for the protection of the Tabasco dikes.

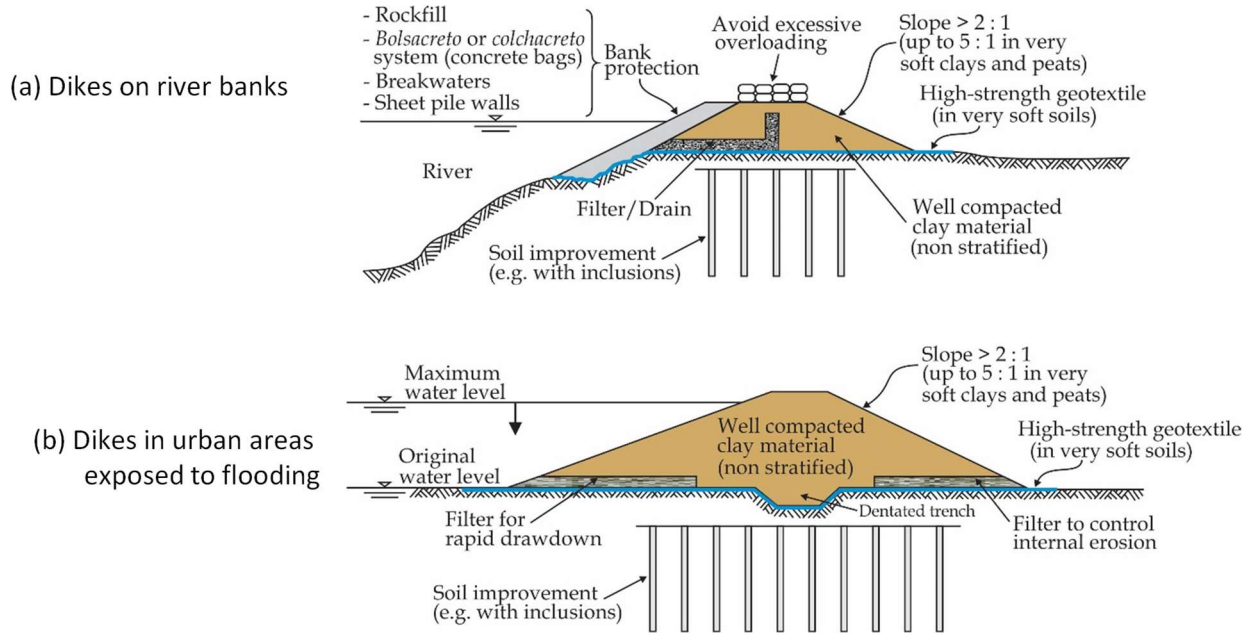


*Figure 10. General recommendations to protect Tabasco dikes*

**CASE HISTORY #2: AGLY RIVER, PYRÉNÉES ORIENTALES, FRANCE**

**Background**

The downstream section of the Agly river (Figure 11) in the Pyrénées Orientales (66) region in France is surrounded by dikes close to its minor bed. This part of the river is 13.2 km long. It is situated in the maritime plain downstream of a mountain area that is prone to intense rainfall: 200 mm in a single day is a common event, and the recorded maximum was 840 mm in 1940.

In 1970, the riverbed was re-profiled and the dikes were built in the current configuration. The protection level is 1250 $m^3/s$, which is a 1/30 annual probability. The presence of abundant vegetation here has a major effect on the discharge and water level rating curve. Safety spillways were included in the initial plan but not built: the dike system is not resilient to overflowing. A dam was built upstream in 1992-1994 to control flooding.

When the river was re-profiled in 1970, the bed was widened to 65-70 m. The dikes generally were constructed to an elevation of 2-3 m, 8 m wide at the crest, with 1V/2H slopes, see Figure 12 and were built using local material. Thus, the materials used vary along the dikes and may consist of loam and sandy loam or even gravel. There is riprap toe protection on the river side, and armour protection over the full height on the concave side of curved sections, as shown in Figure 12b.

In recent years, these dikes have been impacted by major floods which, in some cases, resulted in damage and breaches: specifically, in September 1992, November 1999, November 2005, January 2006, March 2013 and November 2014. The damage during each of these events is described in detail below.

The dikes were first managed by an association of private owners and then by an association of local authorities. Since the introduction of new French regulations on the safety of hydraulic structures in 2007, the regional authority, the *Conseil Départemental des Pyrénées Orientales,* has been in charge of dike management and the fulfilment of regulatory obligations such as inspections, assessments, risk analysis etc.

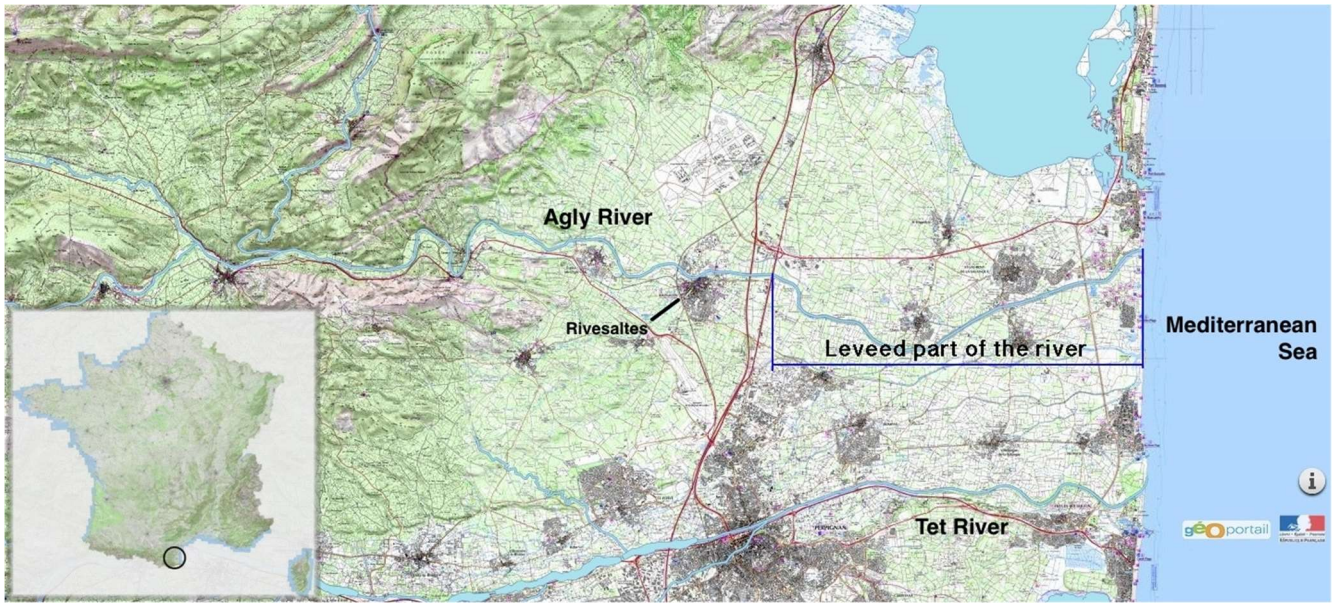


*Figure 11. Location of the lower Agly River (source: IGN Geoportail)*

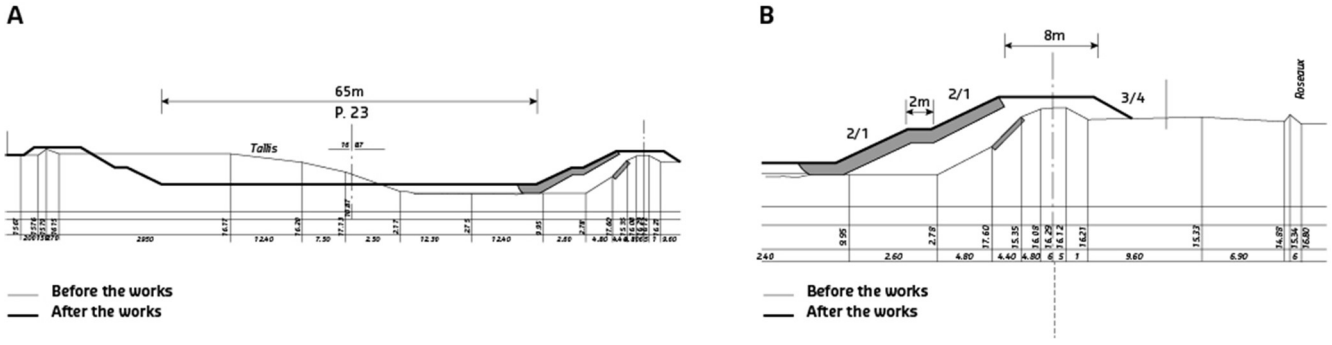


*Figure 12. a) Re-profiling of the river and construction of the dikes, b) armouring of the river side of the dikes in concave sections*

**The September 1992 Event**

This flood was before the construction of the dam. The water level reached the full capacity of the dikes (about 1300 $m^3/s$) but there was no overtopping or breaching. There was some instability, shallow sliding planes along the river side slope caused by drawdown and repairs were made. The annual probability of this event was estimated at about 1/20.

**The November 1999 Event**

The upstream dam managed to contain the entire flood in its catchment area: about 40% of the total catchment and overflowing from the river bed was upstream of the diked section. Even given this reduction in discharge, the flood in the

lower part of the river was still the highest since the dikes were built. The annual probability of the event was estimated at 1/100, with 2000 $m^3/s$ at Rivesaltes. The dikes were submerged: ten places were identified with an overflow head of 20 to 30 cm for about two or three hours. There was severe damage as a result of overflowing, but also owing to internal erosion, external erosion and instability. The event obviously exceeded the design level of the dikes.

Detailed reporting of the damage can be found in CEMAGREF (2000). There was a breach near a sewage treatment plant that was attributed to the general overflowing. It is possible that the presence of a pipe beneath the dike caused the breach here rather than any other element of the system. In many places, the landward side of the dikes was completely eroded due to overflowing and erosion was only stopped by the road revetment on the crest. There was internal erosion in some places as well, as shown by some sinkholes and subsidence on the crest or traces of sand boils in the land alongside the dikes. These internal erosion problems were mainly in the foundations but they were also observed in the dikes themselves: some seepage through the dike was also observed in areas where there were either intersecting pipes or old structures (rocks, wall) inside the dike.

Works after the event included repairing the breach, repairing the eroded land slope (with drains and compacted fill) and repairing the damaged toe protection. Some non-exhaustive work also took place to prevent leakage (masonry on the river side) and sand boils (drainage and seepage system) in different places for each of the problems.

**The November 2005 Event**

Flooding was moderate on this occasion – 1000 $m^3/s$ at Rivesaltes – and very short in duration; the water level almost attained the full capacity of the dikes. Some damage was reported (a lot less than in 1999) but not described in detail in a comprehensive report. Most of the damage was attributed to internal erosion. However, it should be noted that, in the descriptions of damage and its attribution to the different mechanisms between 1999 and 2005, cracks were attributed to instability in 1999 and to internal erosion in 2005. It is entirely possible that both mechanisms were involved, at least in some cases. Furthermore, some seepage was observed at the repaired area of the 1999 breach, probably due to the difficult conditions which meant that the repairs were only reliable for a shorter period of time. There was also mild, local, overtopping.

**The January 2006 Event**

This was also a moderate event: about 800 $m^3/s$ at Rivesaltes. However, it lasted longer: 18 hours rather than the 12 hours in the November 2005 event. The dikes were loaded up to 1/2 to 2/3 of their height. CEMAGREF quickly conducted an inspection of a section of 500 m which had been identified in 1999 as being prone to sand boils. A recommendation had been made to install a drainage and seepage system on the landward side. Some of this work had been completed in 2000 with supervision from the managing authority at the time (an association of local authorities). During the winter of 2004-2005, the landward side of the dike was reinforced with concreted riprap to render it resilient to overtopping. During the 2006 event, a section of 130 m in the same location suffered damage caused by internal erosion in the form of sand boils (Figures 13a, b) and subsidence over a strip of up to 1-2 m wide in the protected plain close to the dike, including the maintenance track, and cracking of the concreted riprap (Figures 13c, d).


*Figure 13. a) Sand boil (photo: Pierre Philippe, CEMAGREF), b) Multiple sand boils close to the maintenance track on the landward side of the dike (photo: Patrice Mériaux, CEMAGREF), c) Damage to the dike itself: cracks on the crest and in the riprap landside revetment (photo: Pierre Philippe, CEMAGREF), d) Damage to the dike itself: crack on the crest; this picture was taken in 2013 but similar damage occurred in 2006 (photo: Patrice Mériaux, Irstea).*

**The March 2013 Event**

The discharge during this event is also estimated to have been approximately 1000 $m^3/s$. There was a breach over a 75-m section in one of the areas prone to sand boils (Figure 14a). The dike itself was eroded, as well as its foundations down to the depth of the minor river bed. The exact cause of the breach is not known because there were no eyewitnesses close to the dike at the time of the breach initiation about 2 hours after the maximum discharge. The breach may have been caused by internal erosion in the dike or the foundation soils, with possible local overtopping following internal erosion and collapse. A large sinkhole was found close to the breach (Figure 14b). Significant additional damage was observed as a result of overflowing (Figure 14c), internal erosion and foundation instability (Figure 14d), as well as internal erosion in the dike itself at one location.

**The November 2014 Event**

Another flood with about the same level occurred on 30 November 2014. There was overtopping in some places along the dike, particularly upstream because of the maximum discharge and downstream because of the high sea level. In the area between, the water level was about 0.5-1 m below the crest level. There was damage as a result of overtopping, external erosion on the landward side caused by intense rain and runoff, and external erosion on the river side caused by the river flow. Like in all the previous events, sand boils and sinkholes were observed in the areas prone to these mechanisms. Detailed reports on the damage and analyses were drafted by the manager, CD66, and its consultant engineer, ISL. Irstea was involved in the analysis of the sand boils and other internal erosion phenomena (ISL, 2014).


*Figure 14. a) The March 2013 breach at the Pia location on the right of the river (photo: DREAL Languedoc-Roussillon), b) A sinkhole close to the breach (photo: Patrice Mériaux, Irstea), c) Damage caused by overflowing (photo: Patrice Mériaux, Irstea), d) Damage to a track on the landward side of the dike caused by under-seepage (photo: Patrice Mériaux, Irstea)*

**Lessons Learned**

Because all these events occurred in a short period, it is now possible to present some lessons learned from the damage and the action taken subsequent to the events.

*Management*

The current management organisation has been in charge of the dikes only since the new French regulations on hydraulic structures came into effect in 2007. The previous management organisations had limited resources. The current organization arranges regular inspections, particularly after flood events and with the aim of compiling information about the dikes, their problems and history. It completed a diagnosis that led to emergency repair works and has also scheduled major upgrades starting in about 2020 on the basis of a risk analysis report (ISL, 2014) to prevent the recurrent problems faced by these dikes.

*Hydrology and Hydraulics*

An update on hydrology and hydraulics has been produced which concludes that the dikes now have a very limited safety level of 1/10 annually, which is not in line with the estimates following the initial works and the first floods of 1992 and 1999. This discrepancy can be explained by the hydrological analysis (data and model), as well as by riverbed changes, and vegetation and sediment patterns.

*Investigation and Diagnosis*

Geotechnical studies were conducted during the initial assessment after the establishment of the new organisation, and after the 2013 and 2014 events. In the context of the risk analysis report (ISL, 2014) a diagnosis was made of the possible causes of failure drawing on the many observations of damage during past events and including the results of studies conducted before 2014. The assessment and diagnosis were conducted locally taking local parameters into consideration. The presentation here is limited to the results at the system level for both sides of the river. The two most probable causes of dike failures are erosion by overflowing and internal erosion of the dike or, more probably, of its foundations. For each of these mechanisms, the conditional probabilities of failure for a 10-year return period event as well as for a 25-year return period event are about $10^{-1}$ to 1, and 1 for the 100-year event. Instability and external erosion by the river are also possible but the probabilities are much lower: 0.02 for external erosion and negligible for instability in the case of all return period events.

*Internal Erosion and Sand Boils*

There are two sections with recurring sand boils: one 700-m-long section on the left bank and one 500-m-long section on the right bank. There is also a 50-m-long section where there are recurring problems with sinkholes on the crest.
The most specific phenomenon affecting these dikes, or rather the subsoil, is the damage of various kinds associated with seepage and internal erosion: sand boils, subsidence, sinkholes, destabilisation of the dike and/or its revetment. These phenomena are found in the literature and in other areas, but they are observed here at high concentrations, and during relatively short floods (typically 1 day) and at low hydraulic heads. Some sand boils were observed inside the protected area up to 40 m from the dike foot, indicating that the gradient is very low. The repairs made until now have been very localised and they did not succeed in solving the problems completely. The general geotechnical model consists of two sub soil layers; a cohesive and impermeable layer at the surface which overlays a non-cohesive and permeable layer, generally sandy loam above sand in the case of the Agly river dikes. Consequently, before erosion can progress in the lower foundation, there must be an initiation mechanism in the surface layer allowing water to flow through it and progress upstream towards the river side. Classically, these initiation mechanisms can heave, uplift or liquefy during the event, or due to initial fissuring (FloodProBE, 2012). It is not clear in this particular case, even after the studies following the latest events, which mechanism or mechanisms are involved. Laboratory tests are presently ongoing. The phenomenon in the permeable and non-cohesive layer could be regressive erosion in the case of sand or suffusion in the case of sandy gravel. The cumulative effect of internal erosion under the dike, whether suffusion and/or regressive erosion, should also be taken into consideration.

**Conclusions and Further Action**

All previous repair works and maintenance works were conducted with a short-term objective given the urgent need to restore the dikes to their previous condition and provide protection during a subsequent event. The levels of protection afforded by the dikes were not adapted to the current situation in the protected area: in the 1970s, the dikes served mainly to protect agricultural land, but there has been extensive urbanization in this coastal area since. Major reinforcements will therefore be required in the next few years on the basis of a detailed design study taking into consideration the results of the recent studies, assessments and diagnosis. This project will include:

- safety weirs in the upstream section of the dike system designed to withstand overflow and to relieve the downstream section;
- raising the crest of the dikes, in sections prone to overflowing to the level required for a $10^{-3}$ annual flood probability including a safety margin;
- removing the dikes from the direct contact with the river bed and building maintenance tracks.

The specific solution in the areas prone to sand boils will take into account the analysis of the efficiency (or lack of efficiency) of previous repairs. It is not possible to provide further details about this issue given the fact that investigations, diagnosis and research are still in progress and also given the legal issues relating to those repairs.

Research including testing and modelling will continue on the materials in order to better understand, characterize and model the specific mechanisms and scenarios (initiation, continuation and progression) responsible for the sand boils and other types of damage seen on the landward side of the dikes.

## CASE HISTORY #3: ADIGE RIVER, ITALY

### Background

The Adige River is the second longest river in Italy (415 km), with a catchment area measuring approximately 12,000 km$^2$. It begins in the Venosta valley in the South Tyrol region and flows across the northeast of Italy before entering the Adriatic Sea (Figure 15). The dike failures discussed here were located in the area of Neumarkt in the South Tyrol, which is within the jurisdiction of the Autonomous Province of Bozen.

The flood event in 1981 led to the collapse of a 220-m-long section of the left flood embankment (chainage 124.450 km to 124.670 km) in Laag (Figure 16). At the same time, a scarp with a differential height of 50 cm was formed on a 238-m-long section in St Florian (chainage 122.150 km to 122.390 km), as shown in Figure 16.

### Evidence of Failure Mechanism

The river level at Laag and St Florian was derived from hydrometer measurements upstream (Branzoll hydrometer), assuming a uniform flow between the section where the hydrometer was installed and the sections where the embankment instabilities were located. The river level computed during the flood event is shown in Figure 17 and 19. At its peak, the river level in Laag and St Florian was still approximately 50 cm below the crest of the dike (Figure 17). Failure was therefore associated with water flow through the dike and/or its foundations and the collapse involved the instability of the landside bank.

Evidence of water flowing through or underneath the embankment is provided in Figure 18b, c. Ponded backwater often accumulates during a flood event and springs form at the toe of the embankment on the landward side.

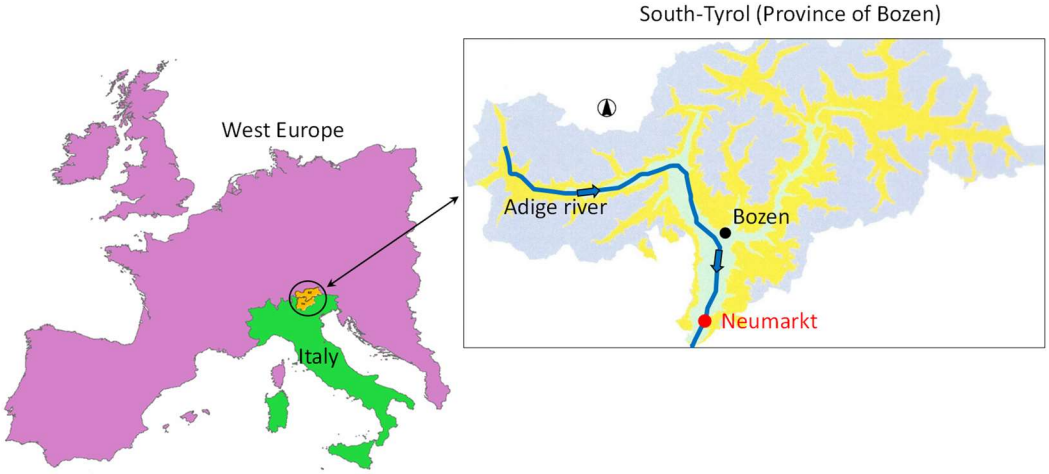


*Figure 15. Map of study area: a) Location of the South Tyrol region; b) Course of the Adige River in South Tyrol and the location of the failure case studies in Neumarkt*

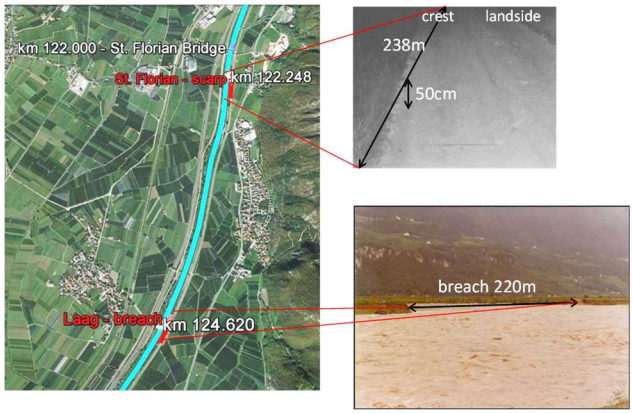


*Figure 16. Overview of the two considered segments of the Adige River at Laag and St Florian*

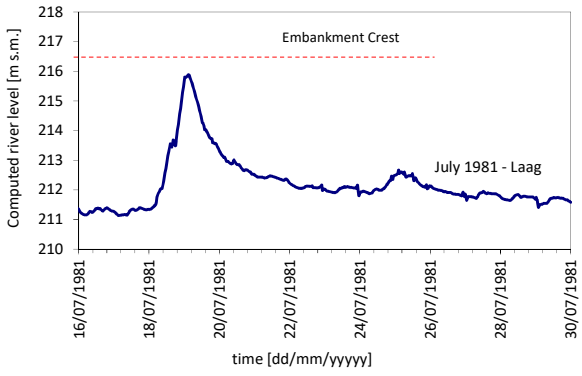


*Figure 17. River level computed at Laag (km 106.185) from 16 July to 30 July 1981. The elevation of the embankment crest is reported as a reference.*

The original riverbed meandered through the Adige valley and was straightened at the end of the 19th century, as shown in Figure 18a, by constructing the current embankments. The ancient river bed is filled with material that is coarser then the surrounding clayey and silty deposits. At some places the current riverbed intersects the ancient river beds and locally the embankments are founded on the coarse-grained filling. As a result, the hydraulic conductivity of the embankment foundation at these intersections is relatively high and groundwater flows preferentially through these layers.

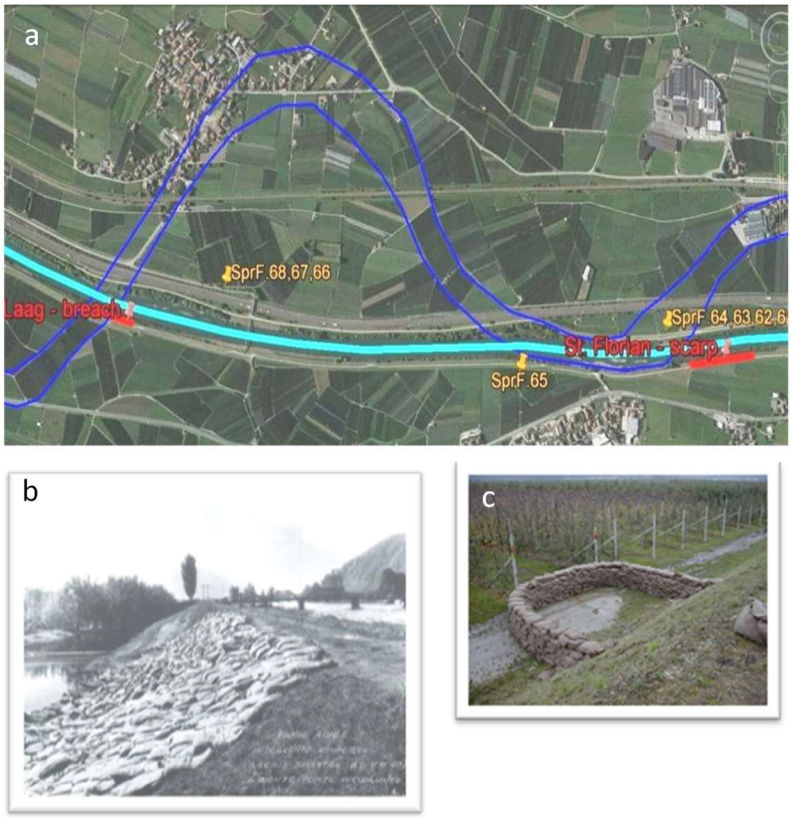


*Figure 18. (a) Current and ancient river bed profiles and spring formation during the flood events in 1997 and 2000 (b) Backwater areas during the 1966 flood (c) Spring formation during the 1997 flood event*

The embankment segment in Laag that was breached in 1981 is actually located on the coarse-grained filling, as is also shown by the borehole logs. On the other hand, the segment in St Florian that was affected by instability, was located slightly outside the ancient riverbed.

Evidence for the collapse mechanisms involving the landward bank can be inferred from the remedial works undertaken on the embankments following the 1981 flood event. In fact, a berm was constructed on the landward side of the embankment to increase the factor of safety with respect to global instability involving the landward bank, Figure 19a and 19b.
During the flood event in 1997, which was even more intense than the one in 1981 (Figure 19c) no collapse phenomena were observed in the segments that had experienced instability in 1981. This can be attributed to the construction of the berm and the increased stability on the landward side.

**Geotechnical Characterization of the Embankments at Laag and St Florian**

The soil profile was characterized using borehole logs, standard penetration tests (SPT) and dynamic probing (DPH) undertaken by the Autonomous Province of Bozen since 1996. The SPTs were in the range $N = 5$ to 35 for the top 12 m. Twenty-two boreholes were used to characterize the embankment segment between chainages 124.000 km and 125.000 km. The SPT profiles were therefore used to confirm the location of the interface between layers. On the other hand, the data from the dynamic probing tests were processed to infer the density of materials forming the embankment and the foundation layers.

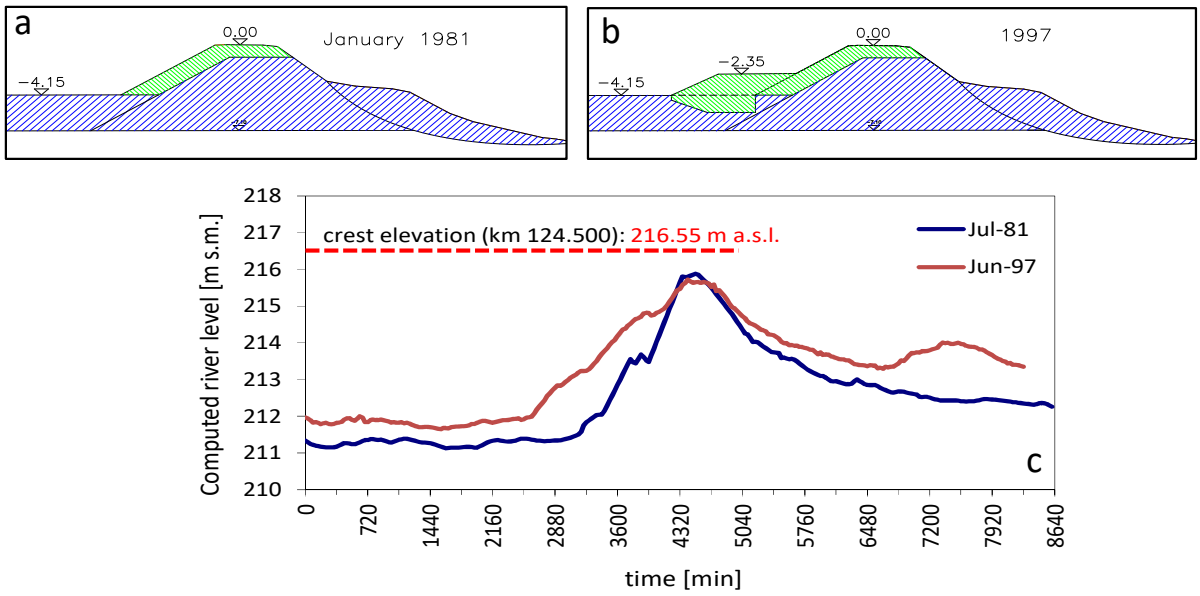


*Figure 19. a) cross section during the flood event in 1981 b) remedial works consisting of a berm on the landward side, c) the river level during the flood events in 1981 and 1997 The elevation of the embankment crest is also reported as a reference.*

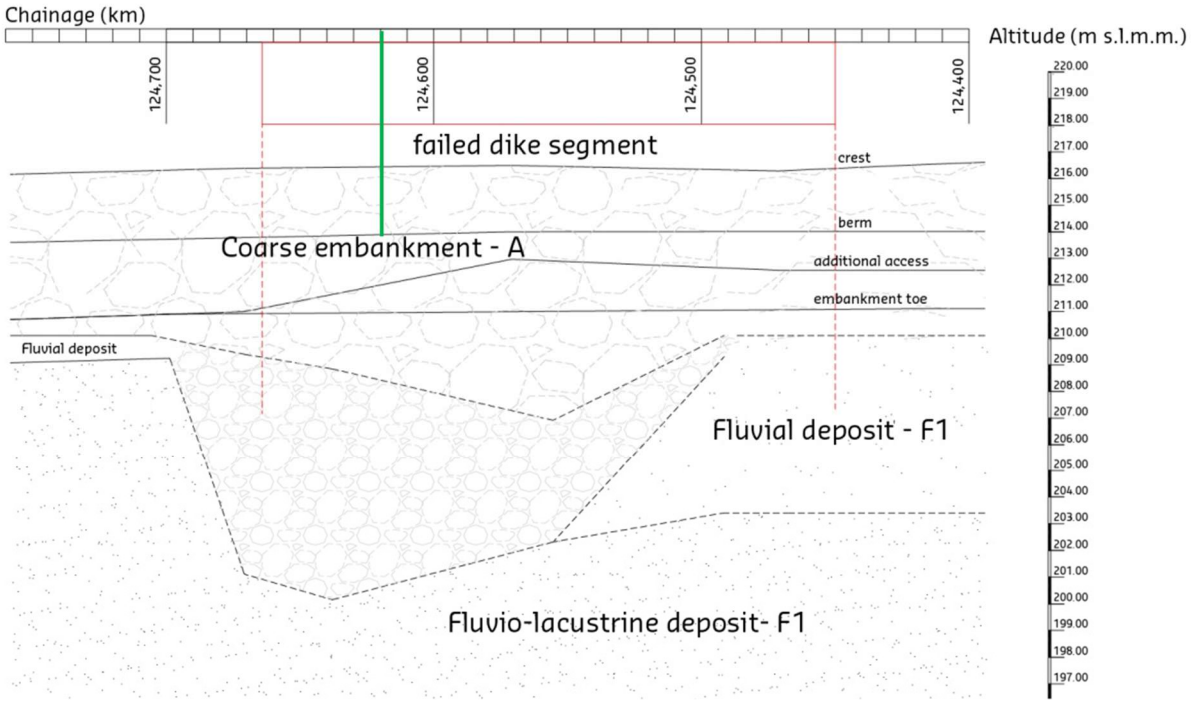


*Figure 20. Longitudinal soil profile of the dike segment in Laag that includes the section breached in 1981. The location of the representative cross-section is indicated by the green line.*

Figure 20 shows the longitudinal soil profile that includes the segment of the dike in Laag breached in 1981 and then reconstructed after 1981. The dip in the interface between the coarse-grained embankment and the ancient river bed is attributable to the excavation of the ancient river bed material after the dike was breached. During the flood, the embankment was patrolled frequently (a few times a day) and no evidence of sand boiling was detected. It is not possible to exclude that

sand boiling was occurring between one visual inspection and another. However, it would appear that failure was mainly caused by underseepage rather than erosion triggered by uplift pressures at the landside toe of the embankment.

The cross-section at chainage 124.620 km was selected to analyze the hydro-mechanical response of the embankment (Figure 21). Figure 22 shows the longitudinal soil profile that includes the segment of the dike in St Florian affected by instability in 1981 (scarp of about 50 cm). The cross-section at chainage 122.248 km was selected to analyze the hydro-mechanical response of the embankment (Figure 23).

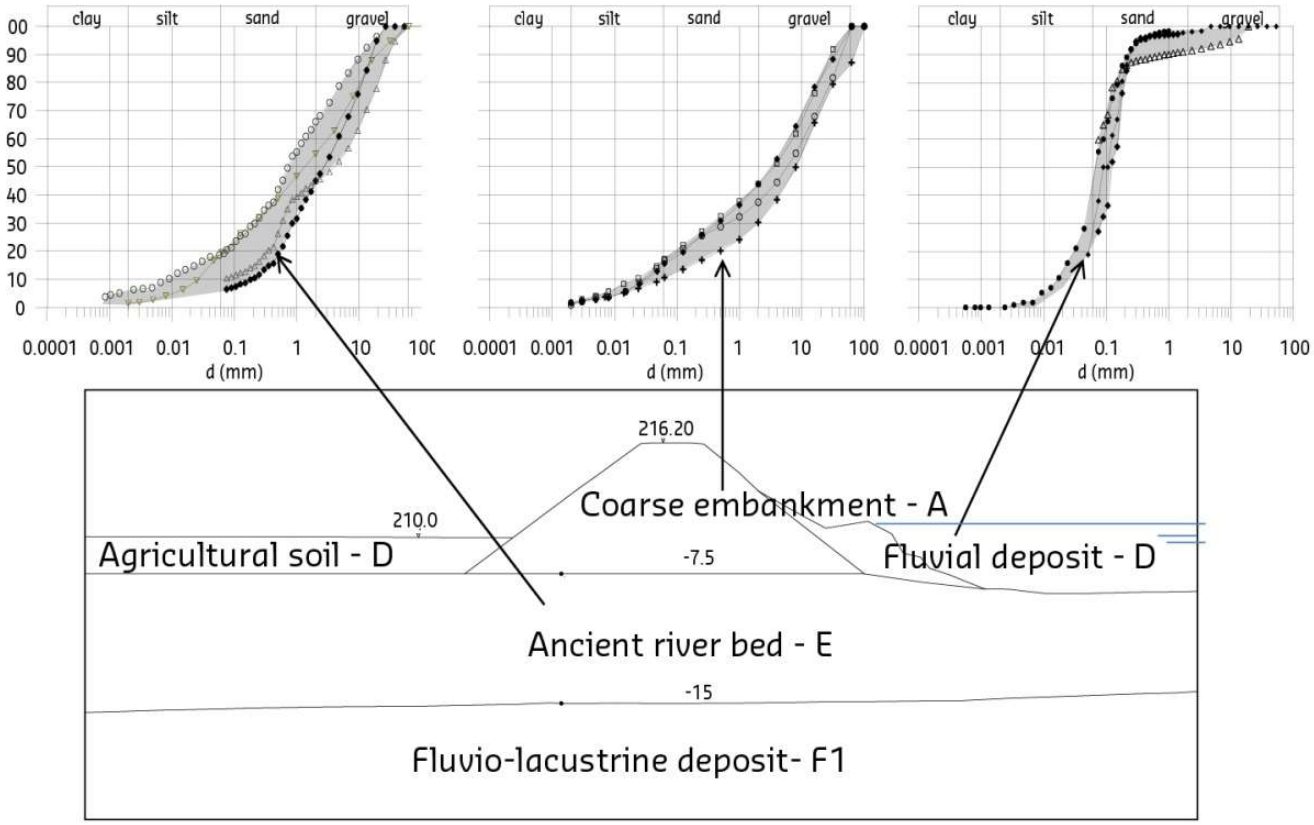


*Figure 21. Soil profile for the cross-section representative of the dike segment in Laag breached in 1981 (chainage 124.620 km)*

The grain-size distribution for the different soil types is shown in Figures 21 and 23, and Table 2. The soil types include:

- A: Embankment coarse soil (well-graded sandy gravel);
- B: Embankment finer soil (well-graded silty sand);
- C: Upper foundation (river sediments formed by silt and sandy silt);
- $F_1$/E: Lower foundation (river sediments formed by sand and gravelly sand ($F_1$) and coarse-grained sediments (ancient river bed, E);
- D: Lateral fluvial deposit (associated with recent flood events, silt).

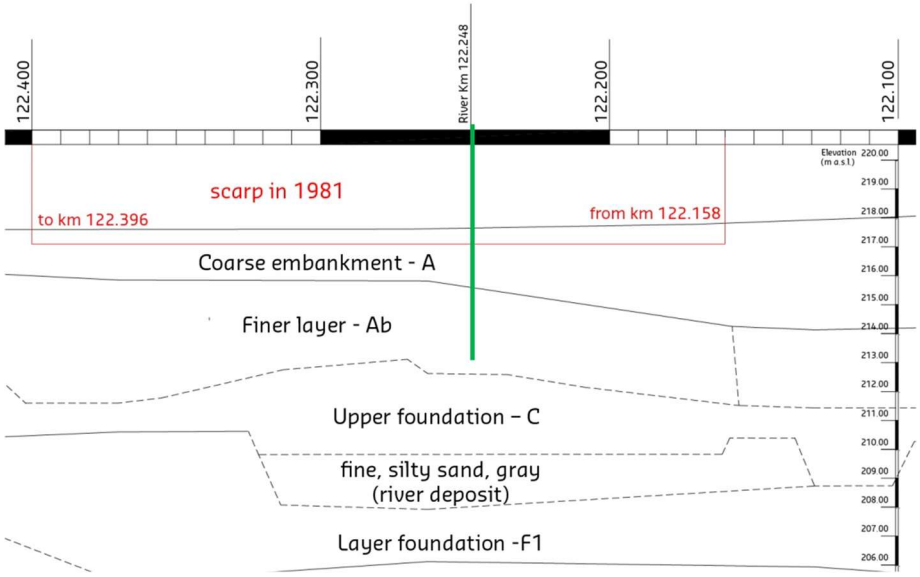


*Figure 22. Longitudinal soil profile of the dike segment in St Florian that includes the portion affected by instability in 1981. The location of the representative cross-section is indicated by the green line.*

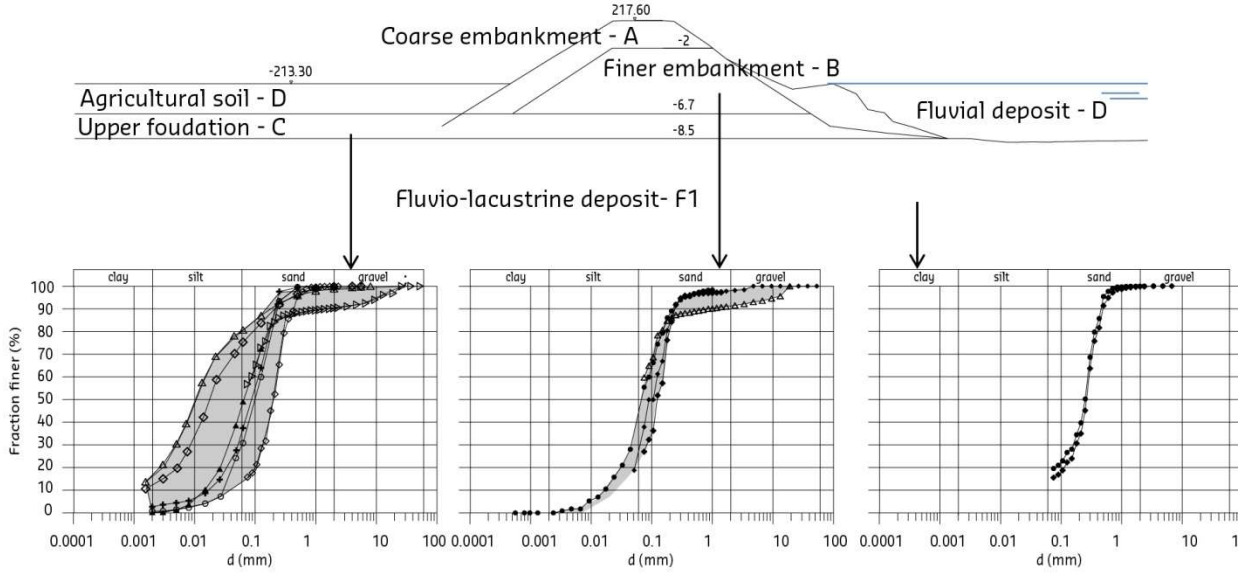


*Figure 23. Soil profile for the cross-section representative of the dike segment in St Florian affected by instability in 1981 (chainage 122.248)*

*Table 2. Soil type and code of the identified layers in the embankment soil profile.*

| Soil type <definition> <UCS classification> | Identified profile layer | | ID code* <letter> <colour> |
|---|---|---|---|
| Coarse material, GW/GM | Embankment: | coarse | A |
| Well-graded silty sand | | fine | B |
| silt, grey sandy silt (river deposit) | Upper foundation (fluvial sediment) | | C |
| medium and coarse sand, SP | Lower foundation | sand deposit | $F_1$ |
| sandy gravel, GM | | ancient river bed | E |
| silty fine sand, sand and silt | Fluvial deposit (cover sediments) | | D |

* As referred to in the geotechnical model

The saturated hydraulic conductivity of the saturated layers, materials C, E, $F_1$, was measured using falling head tests in standpipe piezometers. These measurements focused primarily on the horizontal component of hydraulic conductivity.

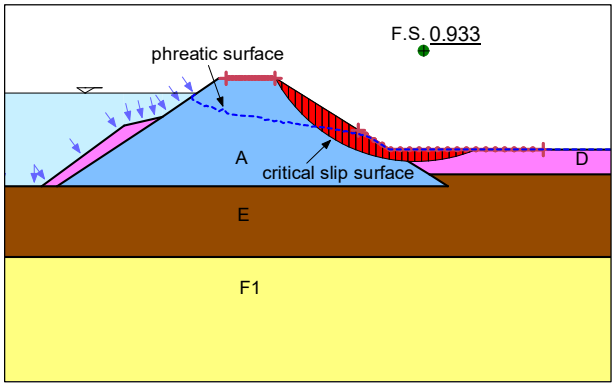


| | $K_{h,sat}$ [m/sec] | $K_v/K_h$ | $\phi'$ [°] |
|---|---|---|---|
| **A** | $10^{-4}$ | 1 | 36 |
| **E** | $10^{-3}$ | $10^{-1}$ | 33 |
| **D** | $10^{-5}$ | 1 | 26 |
| **$F_1$** | $3\ 10^{-5}$ | $10^{-1}$ | 28 |

*Figure 24. Stability analysis and relevant soil parameters at flood peak and transient flow condition of the section at km 124.62 in Laag; c' = 0 kN/m²*

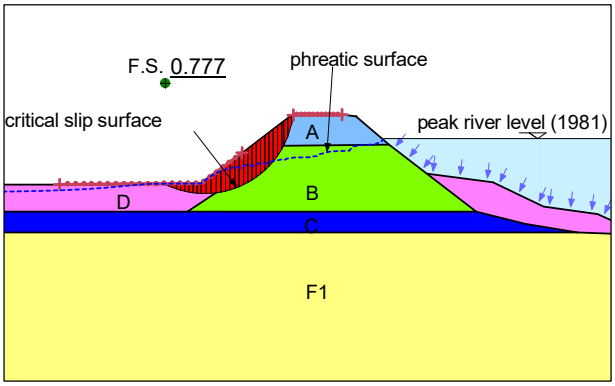


| | $K_{h,sat}$ [m/sec] | $K_v/K_h$ | $\phi'$ [°] |
|---|---|---|---|
| **A** | $10^{-4}$ | 1 | 36 |
| **B** | $10^{-4}$ | 1 | 28 |
| **C** | $10^{-6}$ | $10^{-1}$ | 28 |
| **D** | $10^{-5}$ | $10^{-1}$ | 26 |
| **$F_1$** | $3\ 10^{-5}$ | $10^{-1}$ | 28 |

*Figure 25. Stability analysis and relevant soil parameters at flood peak and transient flow conditions of the section at km 122.248 in St. Florian; c' = 0 kN/m².*

The hydraulic behavior under unsaturated conditions, which is relevant for the embankment (materials A and B) and the soil layer D, was assessed in various ways. Water retention and hydraulic conductivity in the coarse material in the embankment (A) were investigated in an infiltration column developed specifically for this purpose. An equation was derived for the 'main drying' and 'main wetting' curve (Pozzato, 2009) and a modified Brooks & Corey (1966) model was considered for the unsaturated hydraulic conductivity. The parameters used in these models were determined by the inverse analysis of water outflow at the base of the column in the infiltration column tests (Pozzato & Tarantino, 2014). On the other hand, water retention and hydraulic conductivity in soil layers D and B were derived using the approach proposed by Veerecken et al. (1989, 1992). In this approach, water retention and hydraulic conductivity functions are derived from the grain size distribution and dry soil density. The results are given by Figure 26.

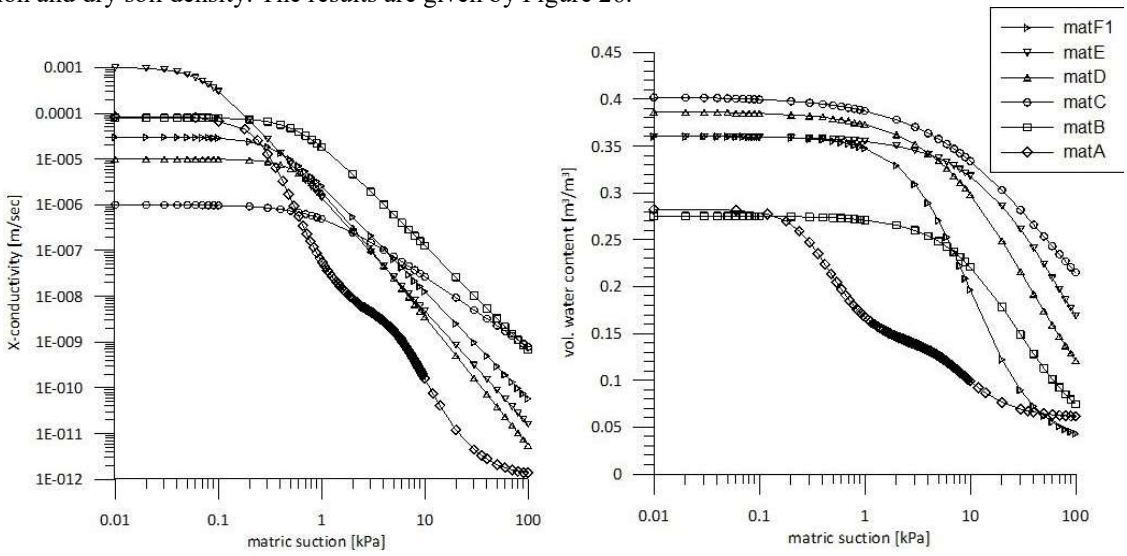


*Figure 26. Hydraulic functions applied in the seepage analysis for saturated and unsaturated zone for each material*

**Results of Numerical Modelling**

The software package GeoStudio 7 was used to model the water flow through the embankment and its foundation and to assess slope stability at various stages of the water flow process. The hydrograph used for hydraulic boundary conditions on the riverside bank was produced as in Figure 17, i.e. by extending the period of 'loading' to the antecedent baseline condition. Boundary conditions were set as follows:

- river level fluctuations applied as constant head on the portion of the boundary 'wetted' by the river;
- right-hand side of the model associated with the river axis of symmetry assumed to be impermeable
- lower boundary of the flow domain assumed to be impermeable
- upper boundary on the landside assigned as 'potential seepage face' boundary.

The initial condition for the transient water flow analysis was generated using a steady-state solution obtained by considering the average river level over the two days preceding the flood event and a constant water inflow from the alluvial fan on the left-hand boundary of the flow domain.

In the stability analyses, the factor of safety and the locations of critical failure surfaces were obtained with the limit equilibrium method (Bishop, 1955) at different times of the transient flow process, including the flood peak.

To this end, the soil mass was discretised into vertical slices delimited by the potential slip surface. The method adopted assumes that the shear strengths of the materials along the potential failure surface are governed by linear, Mohr-Coulomb relationships between shear strength and the normal stress on the failure surface. The analysis provides a factor of safety defined as a ratio of available to mobilised shear resistance. To estimate the soil strength, $\tau$, soil suction is taken into account. The equation (1) proposed by Vanapalli et al. (1996) was considered. The applied values for friction angle, $\varphi$' are given in Figures 24 and 25, while cohesion, $c$' = 0 kN/m$^2$.

$$\tau = c' + \left[ \left( \sigma_n - u_a \right) + \left( u_a - u_w \right) \cdot \left( \frac{\vartheta_w - \vartheta_r}{\vartheta_s - \vartheta_r} \right) \right] \cdot \tan\left( \varphi' \right) \quad (1)$$

where $\sigma_n$ is the normal stress, $\vartheta_w$ is the volumetric water content, $\vartheta_s$ is the saturated volumetric water content and $\vartheta_r$ is the residual volumetric water content. The results of the stability analyses at flood peak for the two cross-sections based on transient flow conditions are shown in Figures 24 and 25. The stability analysis consistently returns factors of safety < 1 for these sections, which proved to be unstable in 1981.

**Concluding Remarks**

Two case studies of embankment failure have been discussed. Instability was caused by water flowing through the embankment and its foundation layers. Evidence of ponding backwater and spring formation during flood events confirms the role of uplift pressure in the instability. The coarse-grained materials forming the foundation layers, especially where the dike intersects with the ancient river bed, favour larger water flows underneath the embankment. Numerical analysis of the water flow under transient conditions and the stability analysis at various stages in the transient process return a factor of safety less than unity, confirming the nature of the mechanisms that are assumed to have controlled the instability phenomena during the 1981 flood event.

**CASE HISTORY #4: RIVER RHINE, BERGAMBACHT, THE NETHERLANDS**

**Background**

The reinforcement of the dike on one of branches of the River Rhine resulted locally in a shortening of the curved path of the original dike over a length of 800 m near the village of Bergambacht, 25 km east of Rotterdam (Figure 27a). This created an opportunity to conduct a field loading test on a cross-section of the original dike.

A typical failure mechanism for dikes in this area is loss of stability due to uplift of the soft soil layers at the toe. Figure 28 explains the failure mechanism. There is a hydraulic connection between the river and the Pleistocene sand layer. A rise in the river level (1) results in an increase in the hydraulic head in the Pleistocene sand layers (2) until the pore pressure equals the weight of the Holocene layers on top (3). The shear strength at the transition between the Holocene clay and peat layers on the one hand and the Pleistocene sand deposit on the other is drastically reduced, creating the conditions for a long, deep, slip plane (4). The uplift phenomenon is described in further detail by Cooling & Marsland (1953), Marsland (1961), Bauduin et al. (1989) and Van (2001). Observations of stability loss due to uplift are scarce and it was decided to study the uplift phenomenon at the Bergambacht test site.

**Soil Conditions and Geometry**

Figure 29 sketches a typical cross-section at the test site. The vertical dimensions are related to *Normaal Amsterdam Peil* NAP, which is approximately mean sea level. The crest height of the dike was NAP +5 m, while the ground level at the toe was NAP 0 m. To facilitate uplift the surface layer was dug away to a depth of 1.8 m over a distance of 70 m parallel to the dike. To prevent a shallow failure mechanism, the distance between the excavated area and the toe of the dike was maintained at 5 m and the excavated area began with a 1:3 slope. The clayey core of the dike body is of medieval origin. Over the years, the dike has been raised and widened and the total height is now 10 m, with a crest height of 5 m above surrounding ground level. The subsoil at the toe of the dike consists of approximately 12 m of peat and clay, followed by a thick Pleistocene sand deposit. Due to the weight of the dike body, the total thickness of the peat and clay layers is reduced to approximately 6 m. More details of the subsoil stratification are given by Figure 30 and Figure 31.

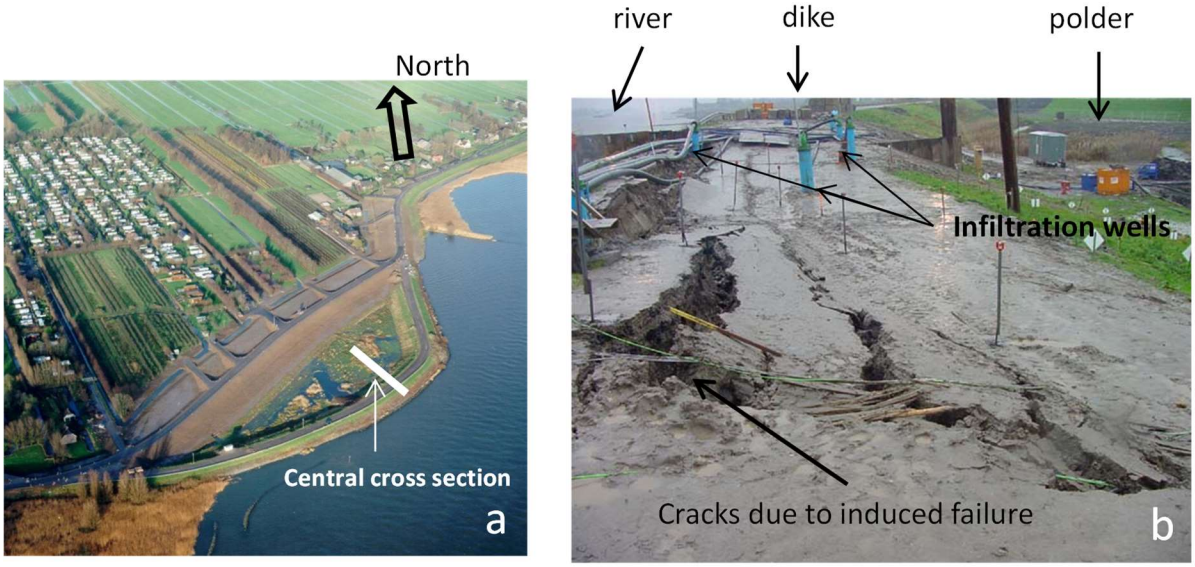


*Figure 27. Test site, a; aerial photograph before testing, arrow indicates North direction, white line indicates the location of the central cross section shown by Figure 29, b; failed dike body after testing*

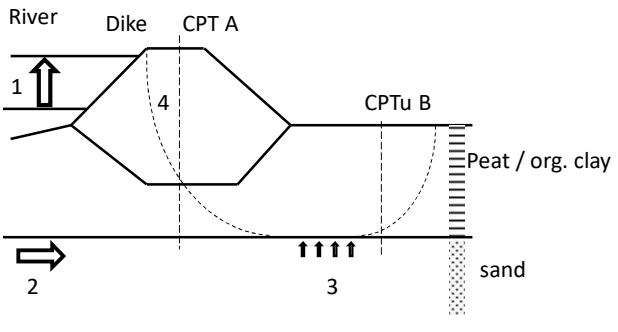


*Figure 28. Impression of the uplift failure mechanism, 1: river level rise, 2: hydraulic connection to sand layer, 3: pore pressure rise until uplift top layer, 4: failure plane.*

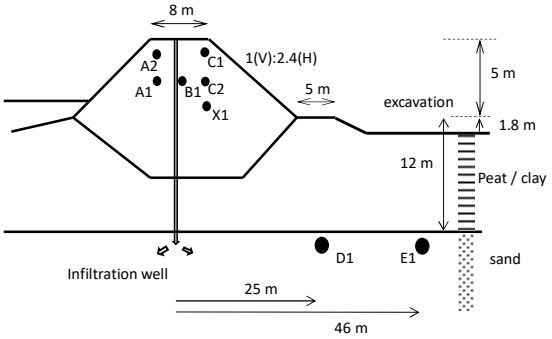


*Figure 29. Test setup and dimensions, A1, A2, B1, C1, C2 , X1, D1, E1 represent locations for hydraulic head measurements shown in Figures 35 and 36.*

Figure 30 and 31 show the subsoil characteristics, based on CPT A, conducted through the crest of the dike and CPTu B conducted at the polder side. The distance between CPT A and CPTu B is 67 m. The interpretation of the CPT A and CPTu B is according to equation (2), (Robertson & Cabal, 2015):

$$q_{net} = q_c + (1-a)u_2 - \sigma_{v0}; \quad s_u = \frac{q_{net}}{N_{kt}}, \quad R_f = \frac{f_s}{q_c} \times 100\% \tag{2}$$

In which $q_{net}$ represents the corrected cone resistance, $q_c$ the measured cone resistance, $a$ the cone factor, here $a = 0.86$, $u_2$ the pore pressure measured above the tip, $\sigma_{v0}$ the overburden pressure, $s_u$ the undrained shear strength, $N_{kt}$ the bearing factor, $R_f$ the friction ratio and $f_s$ the measured sleeve friction. In the application of equation 3 $N_{kt} = 16$ is applied. The friction ratio, $R_f$ is used to identify the transition between the different subsoil layers. The volumetric weight, $\gamma$, presented in Figure 30 represents the mean value assessed from volumetric weights obtained from specimen tested in the laboratory. The volumetric weight given by Figure 31 follows from borehole measurements in which volumetric weight was measured at a 20 cm depth interval. The distance between the CPTu B and borehole is approximately 1 m. For CPT A the pore pressure measurement was omitted and therefore the correction for $u_2$, according to equation 3, was not applied.

It should be noted that the subsoil, found at the location of CPTu B between NAP – 7 m and NAP – 12 m consists of a succession of organic and silty clay layers. For clarity reasons, Figure 31 does not identify these layers individually.

The undrained shear strength profile found by CPTu B shows a dry crust at the top with a thickness of 1.5 m. Below the dry crust, the assessed undrained shear strength ranges mainly between 10 and 20 kN/m$^2$. A Pleistocene sand layer is found at NAP – 12 m. The top 9 m found by CPT A (Figure 30), represent the dike body. The peat and clay layers below the dike body show an undrained shear strength in the range of 40 to 50 kN/m$^2$. This range in $s_u$ is clearly larger than found for the peat and organic clay layers by CPTu B. The difference in $s_u$ found at CPT A and CPTu B can be explained by difference in stress level caused by the presence of the dike body at the location of CPT A.

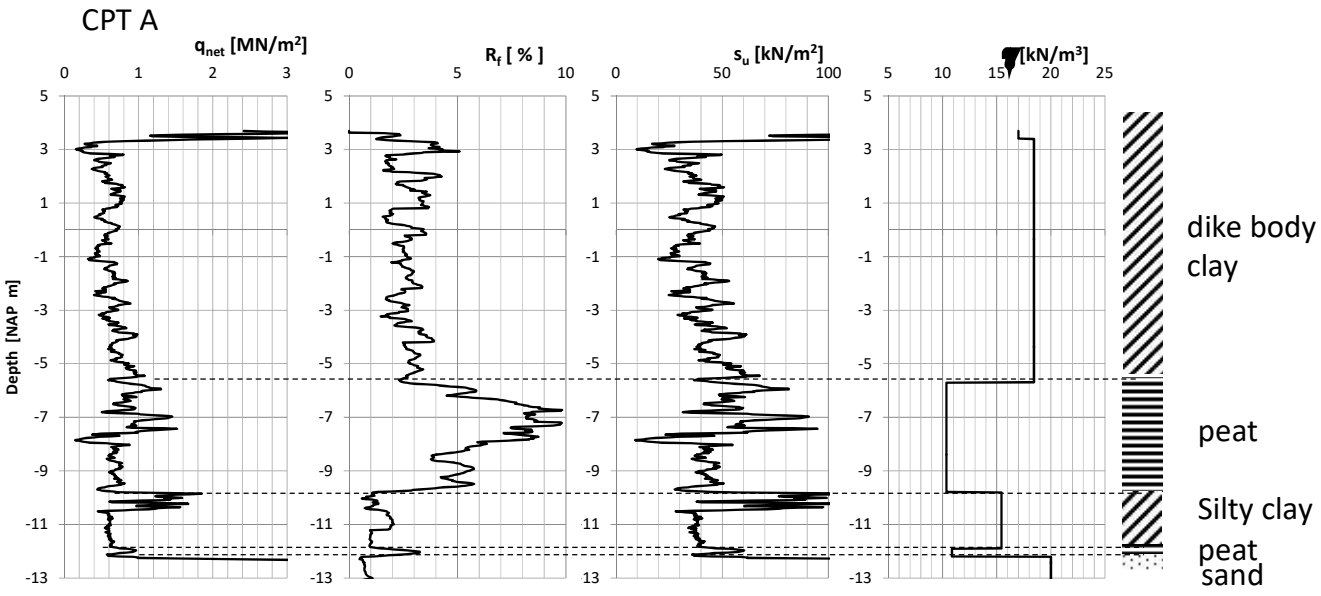


*Figure 30. Depth profiles of corrected cone resistance, $q_{net}$, friction ratio, $R_f$, undrained shear strength $S_u$ for CPT A, crest location (see Figure 28) and average unit weight $\gamma$.*

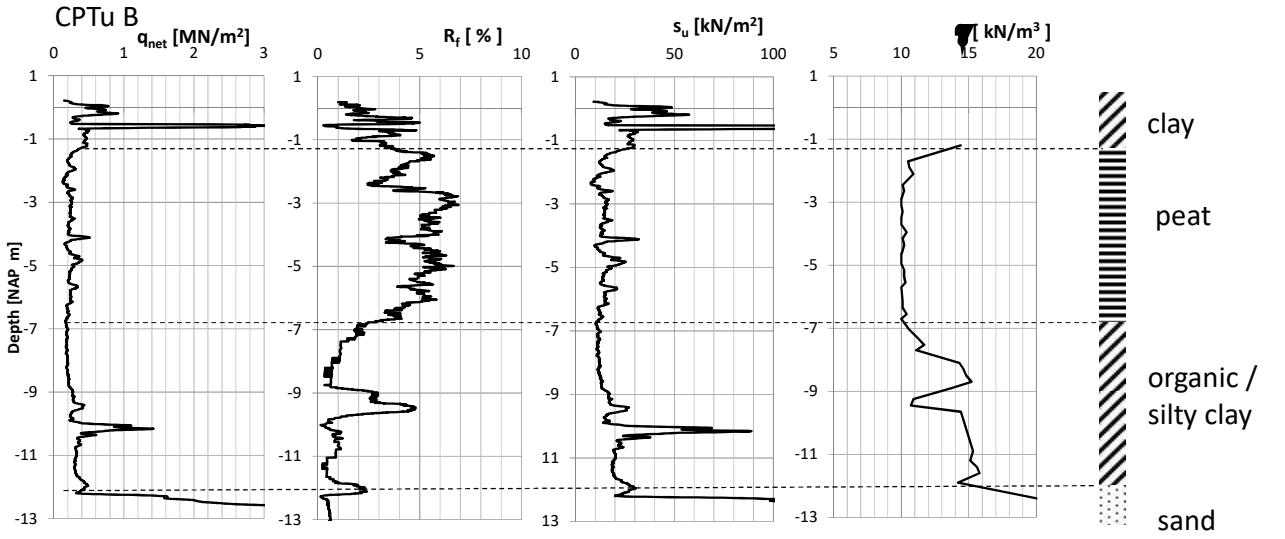


*Figure 31. Depth profiles of corrected cone resistance, $q_{net,}$, friction ratio, $R_f$, undrained shear strength $S_u$ for CPTu B, polder side, location (see Figure 28) and unit weight γ from nearby borehole.*

**Test Setup**

The test is described extensively in Lindenberg et al. (2006). The hydraulic head in the sand layers was raised mechanically using nine infiltration wells placed at the crest of the dike. The monitoring was concentrated in three rows perpendicular to the dike: a central section and a section to the east and west. Figure 29 shows some of the monitoring devices present in the central section.

The test began at 06.00 on 26 November 2000, $t$ = 0 in the graphs below. Figure 32 shows the river level and the average head in the nine infiltration wells. Infiltration started at $t$ = 370 min, 6 hours after the start of the test. Initially, the hydraulic head in the wells followed the fluctuations in the river level. It should be noted that the test site is close to the sea and that the tidal wave has a pronounced influence on the water level in front of the dike. Although drinking water was used for infiltration, the infiltration wells clogged up after 26 hours, $t$ = 1580 min, reducing well capacity. Due to maintenance, required to regain the full pumping capacity, the hydraulic head was seen to fall between $t$ = 1580 and 2260 min, a period of 11.3 hours (Figure 32). Maintenance was also needed between $t$ = 3090 and 3308 min, a period of 3.6 hours. Failure was observed at $t$ = 3450 min, approximately 2.5 days after the start of the test, in the form of large longitudinal cracks in the dike body accompanied by major subsoil deformation (see Figures 33 and 34). The difference in height at the location of the cracks increased to more than 1.0 m (Figure 27b).

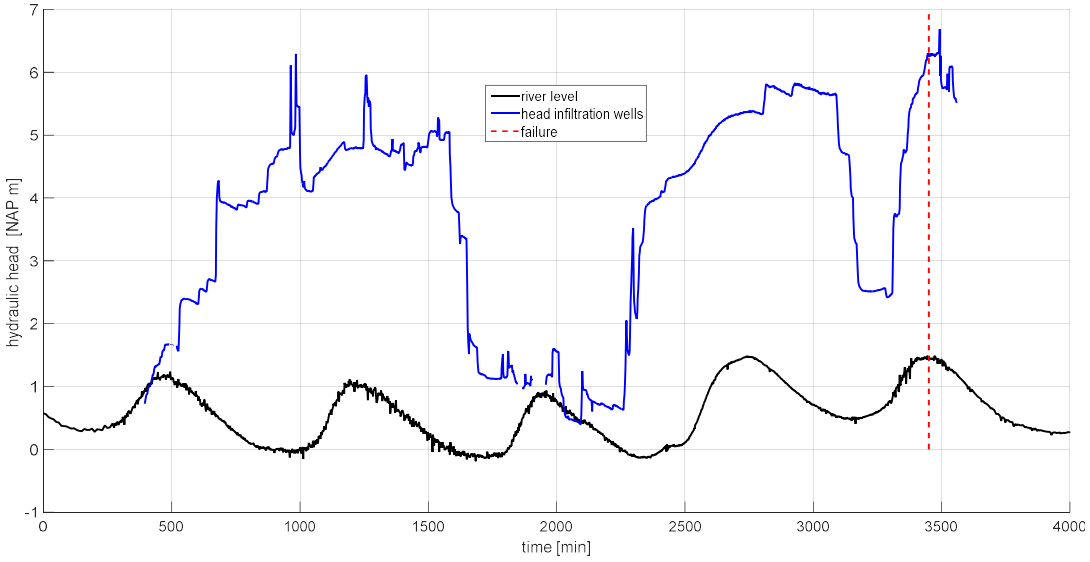


*Figure 32. River level and hydraulic head in infiltration wells during the test*

**Measurements**

Figure 33 shows the horizontal displacements measured at the toe in the eastern and western sections at $t$ = 3300 min (55 h) and $t$ = 3600 min (60 hours). Note that there was no inclinometer in the central section. The maximum displacement was found at the transition between the Pleistocene and Holocene layers, which was not at the same depth in both sections. Figure 34 shows the development of the maximum displacement for both sections. In the western section, horizontal displacements started to develop as soon as infiltration began. At approximately $t$ = 1500 min, infiltration was suspended temporarily and no further deformation was observed until $t$ = 2500 min, when infiltration resumed. Soon after, horizontal displacement developed in the eastern section as well. Infiltration was suspended for a second time, and horizontal displacement stopped again. Soon after infiltration resumed, displacement accelerated until the dike failed at $t$ = 3450 min (57.5 hours) after the start of the test.

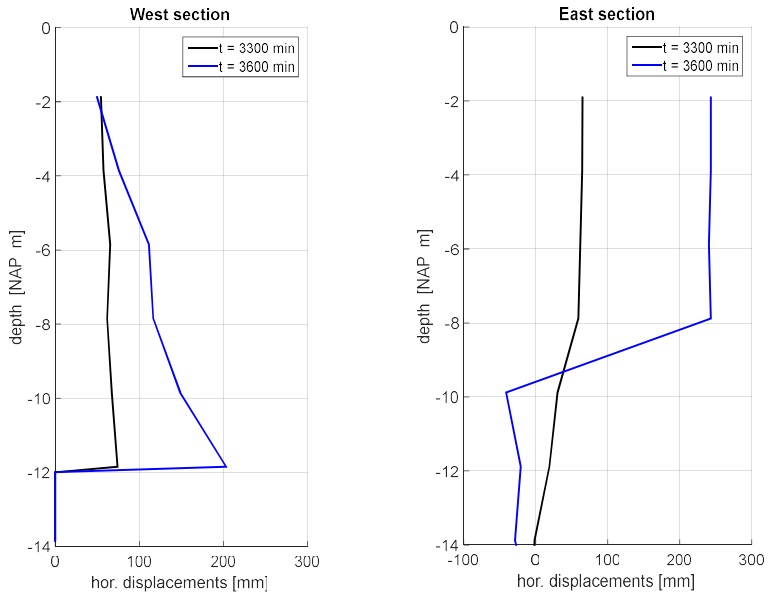


*Figure 33. Horizontal displacement at the toe (both polder-side west respectively east of the central section as shown in Figure 27a)*

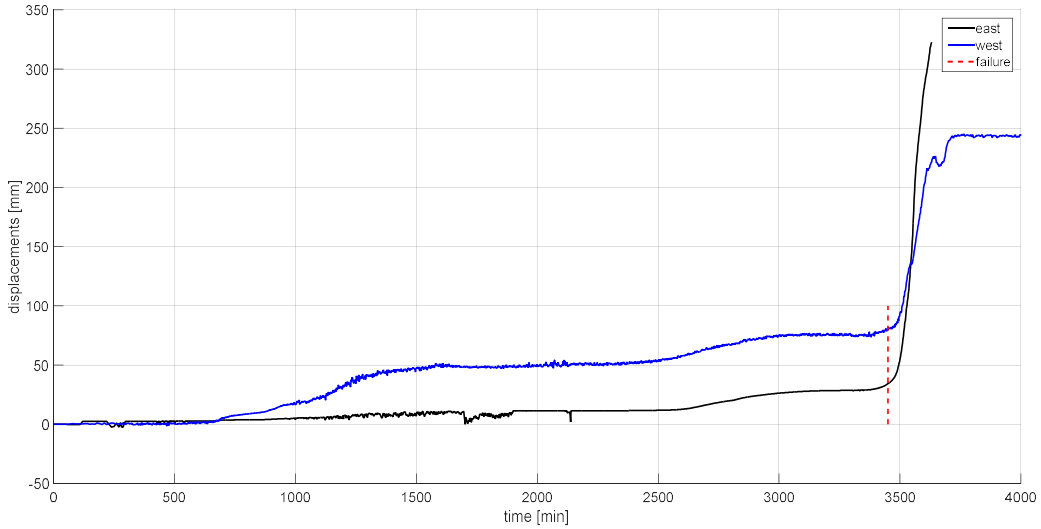


*Figure 34. Development of maximum horizontal displacement during the test*

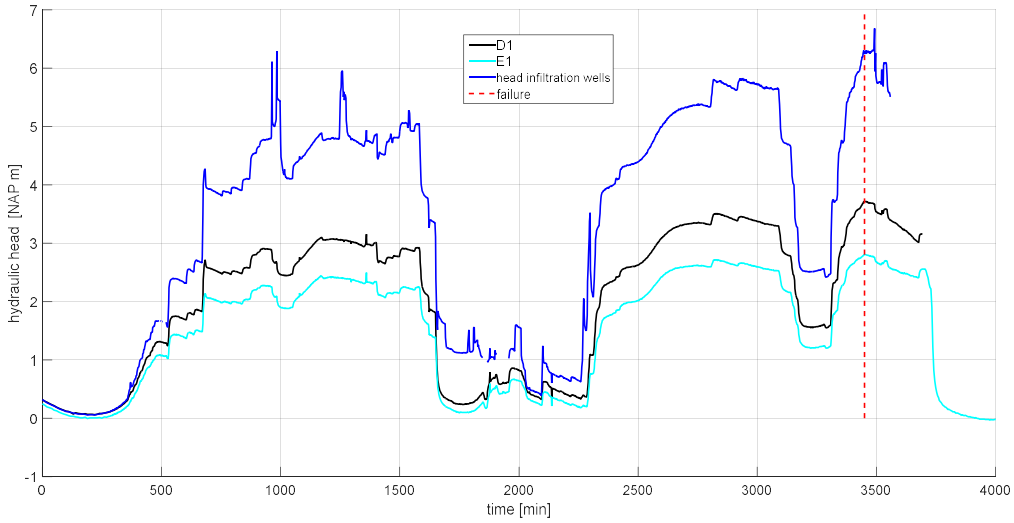


*Figure 35. Hydraulic head in Pleistocene sand layer, locations D1 and E1 (see Figure 29)*

Figure 35 shows the hydraulic head observed in the Pleistocene sand layer at distances of 21 and 42 m from the infiltration wells. The effect of infiltration declined with increasing distance from the well; the hydraulic head at D1 was lower than in the infiltration wells and a further reduction in maximum head was observed in E1.

Figure 36 shows how hydraulic head developed inside the dike body. Prior to failure there was no significant fluctuation in hydraulic head. The range in hydraulic heads measured by the different transducers can probably be explained by suction forces at the top of the dike. With the exception of C2, there was a sharp drop indicating failure. Close inspection shows that, inside the dike body, the response to failure was later than given by the observed horizontal displacement at the toe, $t = 3450$ min at which only the pore pressure at location C2 shows a response. There was a minor initial response at B1 and C1 shortly after $t = 3450$ min. The sharp drop in hydraulic head was observed later. The drop at X1 and C1 was observed at $t = 3595$ min, or 145 min (2.4 hours) later. At $t = 3644$ min (50 minutes later) the hydraulic head at B1 and A2 dropped significantly. The time differences for local failure found at different locations shows the propagation of the failure plane, starting deep in the subsoil and moving towards the crest. It should be noted that the development of the failure plane resulted in breakage of the infiltration wells. When infiltration ceased, the uplift conditions were no longer in place and sliding along the slip plane as indicated by Figure 28 stopped.

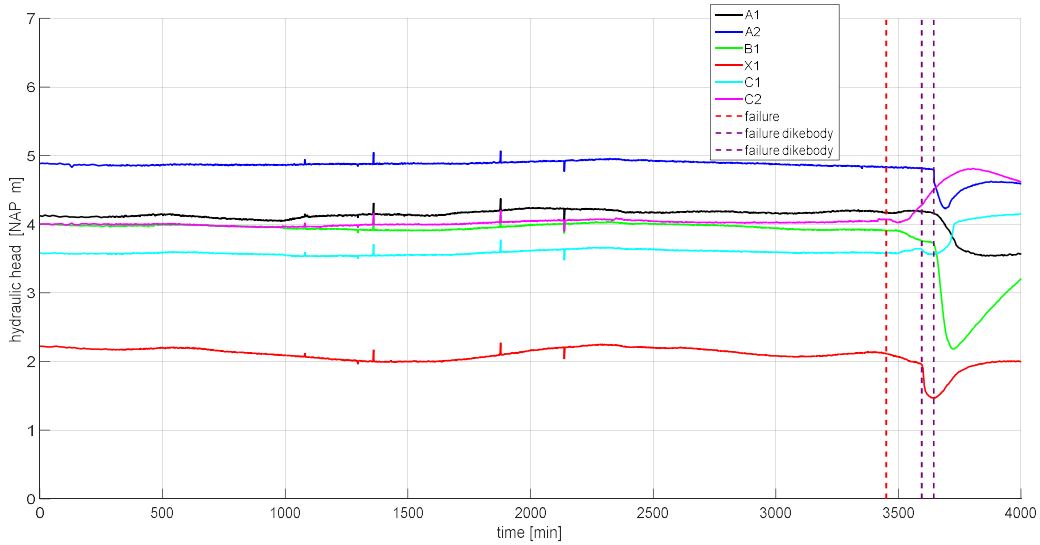


*Figure 36. Hydraulic head in the dike body for locations A1 to C2 (see Figure 29)*

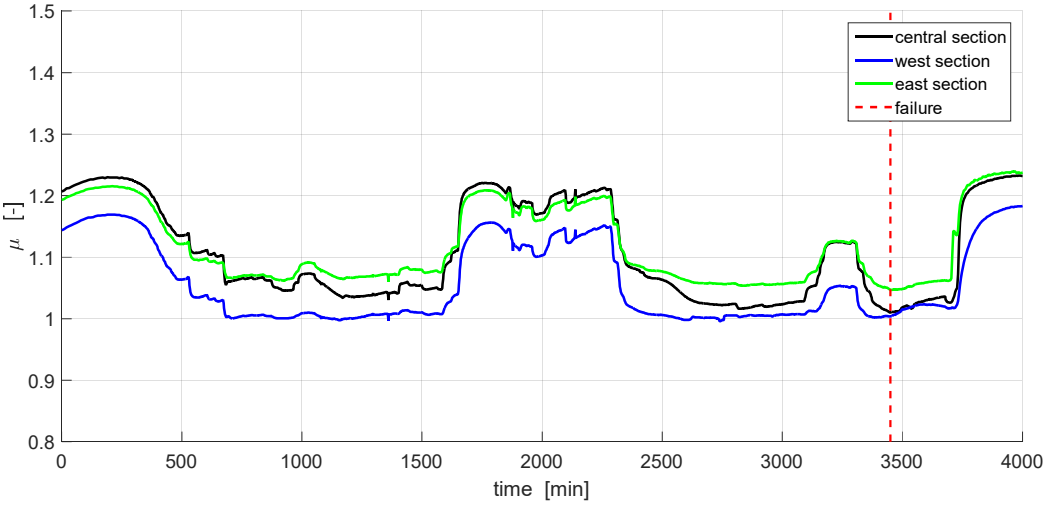


*Figure 37. Ratio of total overburden pressure to pore pressure, $\mu$, during the test*

To check on the uplift conditions during the test, the ratio, $\mu$, of the weight of the Holocene layer to pore pressure in the Pleistocene sand layer was determined for each of the transducers in the Pleistocene sand layer. Figure 37 shows the ratio, $\mu$, during the test for the transducers placed at 46 m from the crest of the dike in the central, eastern and western sections. Initially, $\mu = 1.2$. When infiltration began, this value reduced, as expected. Due to differences in the subsoil layer, $\mu$ varied for the different sections, with the lowest value in the western section, where the value remained approximately 1. In the central and eastern sections, $\mu$ seemed to reduce slightly during the test. This corresponds to the slight increase in infiltration pressure during the test, as shown in Figure 35. The value did not drop significantly below 1.0. This could be explained by the pumping capacity, which does not allow for any further increase in pore pressure in the sand layer at the toe of the dike. It can also be hypothesized that when the pore pressure in the sand layer starts to exceed the weight of the clay and peat layers above it, a gap is created which is filled with pore water from the sand layer until a new equilibrium is attained. When pumping capacity is further increased, the gap may be widened, maintaining the equilibrium in vertical forces. In this hypothesis, $\mu = 1.0$ could be a physical boundary that will have prevented any further decline in the $\mu$ value in the western section during the test. It should be noted that, at larger distances from the dike, the Pleistocene hydraulic head decreased, causing an increase in $\mu$. Close to the dike, $\mu$ is affected by the weight of the dike body.

Figure 33 shows that horizontal displacement in the western section was initially higher than in the eastern section. This corresponds well to the lower $\mu$-value found for the west section, indicating that uplift was reached at an early stage of the test in the western section. The dike was seen to fail when the $\mu$-value reached the lowest level during the test in the central section, $\mu = 1.01$, and eastern section, $\mu = 1.05$.

**Conclusions**

This section briefly presented the Bergambacht field test. It shows that the loss of stability caused by uplift, as shown in Figure 28, is a realistic failure mechanism. The induced failure extended over a large area and reached the top of the Pleistocene sand layer. The dike and subsoil failed progressively, with the first indication of failure found at the deepest part of the slip circle. From there, the failure zone developed until it reached the dike body, as indicated by the pore pressure measurements. The period between the first indication of failure in the deepest part of the failure plane and the failure of the dike body is approximately 3.2 hours. This is considered to be a rapid, undrained failure.

The three monitored sections at the test site showed differences in behaviour, with the western section being the first to fail. This also indicates a lateral propagation of the failure plane, which may be induced by a slight increase in infiltration pressure during the test.

## CASE HISTORY #5: TAGUS RIVER, PORTUGAL

**Background**

This section presents the main failure mechanism of a peripheral dike located very close to the Tagus River delta in the Lisbon metropolitan area. The dike protects the "Mouchão da Póvoa", a fluvial island used for agriculture with an overall area of 1200 ha and 800 ha of dry land that plays a very important role in the Tagus River ecosystem. The dike consists of a clay fill

on an alluvium layer protected on the outer face by riprap (rock armour) revetment. The island has been used for agriculture for at least the last 80 years. Figure 38 provides views of the failure that occurred on March 2016.


*Figure 38. Location and view of the dike failure.*

**Main Constraints**

Given the location of the island in the Tagus River delta, one of the widest estuaries in Europe, the geological scenario is very complex: alluvium deposits, mainly very soft clays, with $S_u$ not greater than 20 kPa, sometimes interbedded with silty and sandy layers, with an overall depth of approximately 30 m (Figure 39). The alluvium rests on the bedrock of Miocene sandstone.

The velocity of the Tagus River reaches up to 3 m/sec, and waves with a height of up to 1 m cause the erosion of the outer face of the dike. The tidal range of the Tagus River is approximately 3.2 m. Due to the high velocity and wave action, a riprap revetment was installed to protect the dike from erosion. However, in recent years, no maintenance work was done on the riprap revetment, leading to its gradual degradation.

**Main Failure Mechanism**

The main failure mechanism is related to the erosion of the clay fill due to water inflow and the mechanical action of the waves on the outer face of the dike. Failure originated with the erosion of the riprap revetment (Figure 39). The presence of a permeable sandy layer below the dike foundations also contributed to the failure mechanism. The actual dike failure began during the severe winter of 2015 - 2016 and involved a section with an overall length of approximately 30 m. When the failure occurred, the water level in the Tagus River was approximately Mean Sea Level, MSL, +4.20 m. In October 2016, the overall length of the dike failure line had increased to approximately 80 m.

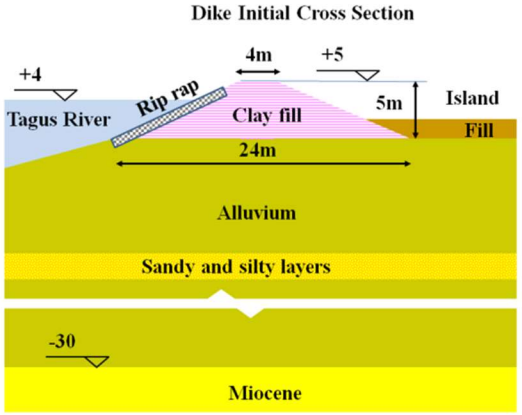


*Figure 39. Initial dike cross-section and geotechnical profile.*

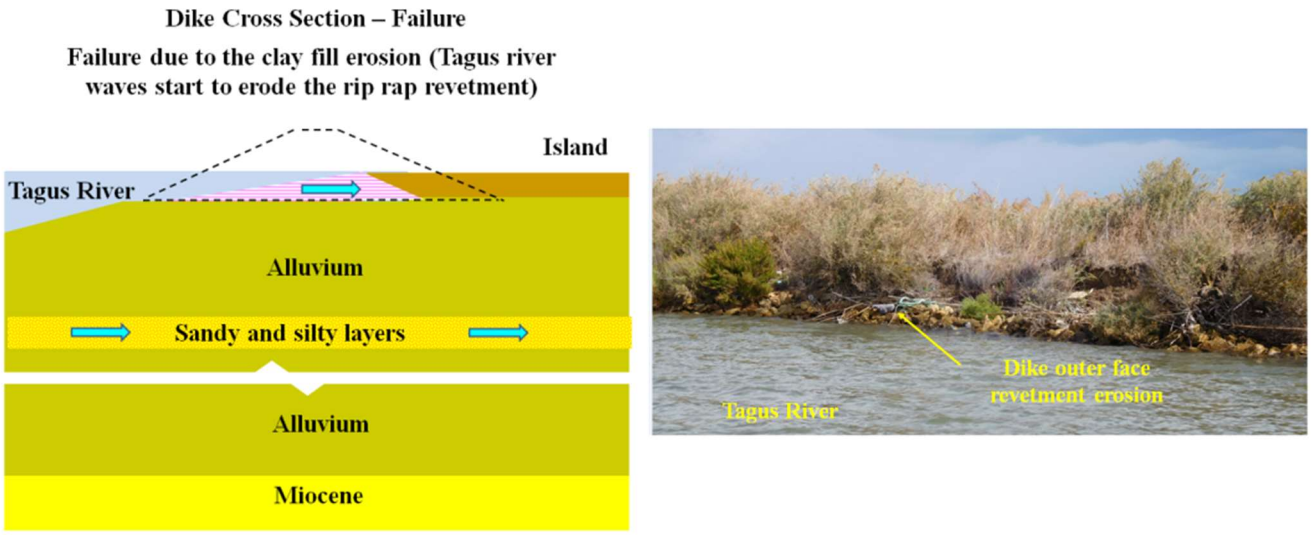


*Figure 40. Dike failure due to the erosion of the clay fill, cross-section and view of the outer face.*

**Adopted Remediation Solutions**

The proposed dike remediation solutions comprised the use of a driven sheet-pile wall braced by inclined driven steel micro-piles, all capped with a top and a central, reinforced, concrete beam. Those works are to be performed from a barge at high tide. The depth of the sheet pile walls will have to be enough to pass through the silty and sandy alluvial layers. A protection and stabilisation fill will be required on both the outer and inner sides of the sheet piling. On the outer face of the fill, a riprap protection revetment will be required to protect the fill from hydraulic erosion. Figure 41 illustrates the reconstruction works.

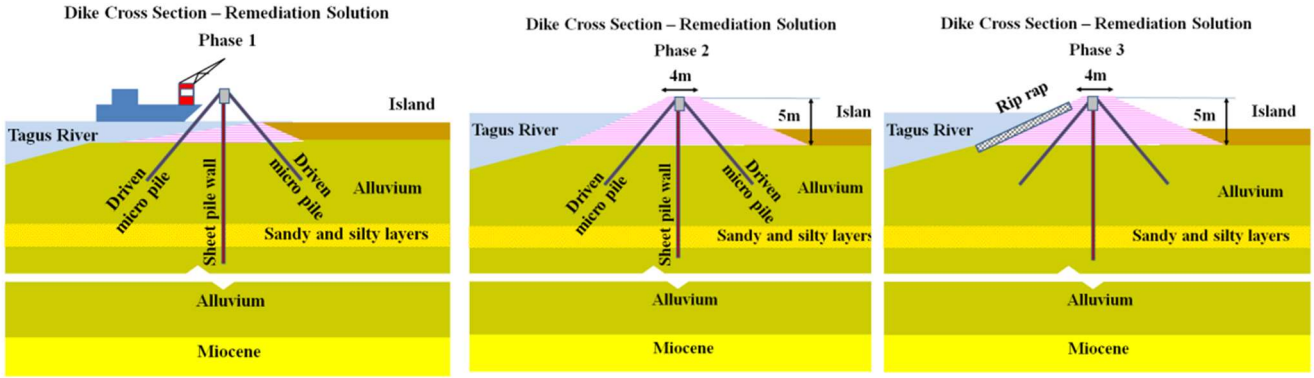


*Figure 41. Dike remediation: main construction phases.*

**Lessons Learned**

The main lesson learned is that the need for preventive maintenance should be emphasised. In this case, the lack of maintenance work on the riprap protection was the main reason for the failure, which was further facilitated by the absence of a suitable geotextile. The installation of a comprehensive monitoring and survey system is also very important. The installation of the monitoring and survey system should be accompanied with a better understanding of the geological and hydrogeological conditions and assessment of subsoil characteristics as strength, stiffness and permeability.

**CONCLUSIONS**

The present paper discussed five different cases of dike failures. The cases illustrate the wide variety of loading conditions and failure mechanisms for dikes. The relevance of the individual failure mechanisms depends on the actual loading and local

subsoil conditions and dike structure. The cases show that the strength of a dike depends not only on the material used to build the dike, but also on subsoil conditions.

In the case of the Tabasco dikes, the erodibility of the dike material itself was the main issue. This case shows how an analysis of the observed damage led to an improved dike design tailored to the local loading conditions. The main failure mechanism in the Agly River case was the erodibility of the subsoil. This case showed how difficult it can be to distinguish between different failure mechanisms. It is not only in the design phase that the calculated factors of safety for different failure mechanisms might be close to one another: field observations do not always clearly identify the types of failure mechanism involved. The Agly river case also illustrates that the impact of flooding depends on the local population density: increases in the local population density should lead to an increase in the standards for flood risk management.

Both the Adige River and the Bergambacht cases demonstrate the importance of understanding subsoil behaviour and hydraulic head development in permeable subsoil layers. In the Adige case, the subsoil mainly consists of granular material. The development of the hydraulic head in the subsoil caused internal erosion that led to dike failure. In the Bergambacht case, the development of the hydraulic head resulted in the uplift of the relatively impermeable clay and peat layers at the toe. The uplift impaired stability and led to a slip-circle failure.

In the Tagus River case, failure was induced by erosion due to wave action. That case demonstrates the importance of regular inspection and preventive maintenance.

## ACKNOWLEDGMENTS

The authors would like to thank:

- the Conseil Départemental des Pyrénées Orientales, the current manager of the dikes, the ISL engineering consulting firm, and Irstea's colleagues Patrice Mériaux and Nadia Benahmed for providing the information on the Agly River case.
- Rijkswaterstaat for initiating and financing the Bergambacht test site.

## REFERENCES

Den Adel, H., Bakker, K.J., and Klein Breteler, M. (1988). "Internal Stability of Minestone.", *Proc. International Symposium on Modelling Soil–Water–Structure Interaction,* International Association for Hydraulic Research (IAHR), Netherlands, Balkema, Rotterdam, 225–231.

Ahlinhan, M. F., and Achmus, M. (2010). „Experimental Investigation of Critical Hydraulic Gradients for Unstable Soils. Geotechnical Special Publication No. 210, American Society of Civil Engineers (ASCE).", *Proc. of the 5th International Conference on Scour and Erosion*, San Francisco, CA, 599-608.

Auvinet, G., López-Acosta, N.P., and Pineda, A. R. (2008). Final report of Integral Hydraulic Project of Tabasco (PHIT) Research Report of Geotech. Department, Institute of Engineering UNAM, Mexico (in Spanish).

Bauduin C.M.H., Moes C.J.M., and van Baalen M. (1989). "The influence of uplift water pressures on the deformations and stability of flood embankments." *Proc. 12th Int. Conf. Soil Mech. Found. Eng.* Rio de Janeiro, Balkema Rotterdam

Berilgen, M. (2007). "Investigation of stability of slopes under drawdown condition.", *Computers and Geotechnics* (34), 81-91.

Bishop, A. W. (1955). "The use of the Slip Circle in the Stability Analysis of Slopes.", *Géotechnique* 5: 7

Brooks, R.H., and Corey A.T. (1964). "Hydraulic properties of porous media.", *Hydrology Paper 3*. Colorado State Univ., Fort Collins, CO

CEMAGREF (2000). Digues de la basse plaine de l'Agly: Relevé et diagnostic des désordres consécutifs à la crue du 12-13/11/1999. Rapport de fin d'études (33 p.) (in French)

Cooling L.F., and Marsland A. (1953). "Soil mechanics studies of failures in the sea defence banks of Essex and Kent.", *Conf. on the North Sea Floods of 31st January – 1st February 1953* p 58-73 London, Inst. Civil Eng.

FloodProBE D3.1. (2012) Guidance on improved performance of urban flood defences, Chapter 2 Internal Erosion (pp. 4-33). http://www.floodprobe.eu/partner/assets/documents/Floodprobe_D3.1_V2_5.pdf (last visited March 2018)

Van Genuchten, MTh. (1980). "A closed-form equation for predicting the hydraulic conductivity of unsaturated soils.", *Soil Science Society of America Journal*, 44(5), 892-898.

GEO-SLOPE International, Ldt (2008). SEEP/W-2007 2008: Scientific Manual: Seepage modeling with SEEP/W, An Engineering Methodology, Third Edition, GEO-SLOPE International, Ldt, Calgary, Alberta, Canada.

IFRCRCS (2016). World Disasters report 2016, International Federation of Red Cross and Red Crescent Societies (D. Sandersen & A. Sharma, eds) ISBN 978-92-9139-240-7.
ISL Ingénierie (2014). Etude de dangers des digues de l'Agly maritime, Report (230 p.), (in French)
Lane, P.A., and Griffiths, D.V. (2000). "Assessment of stability of slopes under drawdown conditions.", *Journal of Geotechnical and Geoenvironmental Engineering* 126(5), 443–50.
Lindenberg J., Van M.A., Koelewijn A.R., Lambert J.W.M., Zwanenburg C., van der Meer M.T., Teunissen P.A.A., and Loos E.C.C. (2006). Evaluation of Bergambacht Field test, GeoDelft report number CO-418012, Translated from Dutch by Vastenburg & v.d. Heijde
López – Acosta N.P., Sánchez M.A., Auvinet G., and Pereira J.-M. (2015). Assessment of exit hydraulic gradients at the toe of levees in water drawdown conditions, *Scour & Erosion, Cheng, Draper & An (eds)* Taylor & Francis group, London, ISBN 978-1-138-02732-9
Marsland A. (1961). "A Study of a Breach in an earthen embankment caused by uplift pressures.", *Proc 5th Int. Conf. on Soil Mech.and Found. Eng.* Paris.
Pozzato, A. (2009). Stability of River Embankment of coarse-grained well graded soil: the case study of the Adige River at Egna (BZ). *Ph.D. Dissertation* at the University of Trento.
Pozzato A., and Tarantino A. (2014). "Characterization of the hydraulic behavior of coarse-grained flood embankment materials.", *Proc. 6th International Conference on Unsaturated Soils: Research & Applications*, Sydney, Australia 2-4 July 2014.
Robertson P.K., and Cabal K.L. (2015). Guide to Cone Penetration Testing for Geotechnical Engineering, 6th edition Gregg Drilling & Testing Inc. http://www.cpt-robertson.com/doc/view?docid=xnhqTpmrnRdPTvYHHRSr6hcNdKJLWy (last visited March 2018).
Van M.A. (2001). "New approach for uplift induced slope failure.", *Proc 15th Int. Conf. Soil Mech. Geot. Eng.* Istanbul.
Vanapalli, S.K., Fredlund, D.G., Pufahl, D.E., and Clifton, A.W. (1996). "Model for prediction of shear strength with respect to suction.", *Can. Geotech. J.,* vol. 33, pp 379-392.
Vereecken, H., Diels, J., Van Orshoven J., Feyen, J., and Bouma J. (1992). "Functional evaluation of pedotransfer function for the estimation of soil hydraulic conductivity.", *Soil Sci. Soc. Am. J.* 56: 1371-1378.
Wan, C. F., and Fell, R. (2004). "Investigation of Rate of Erosion of Soils in Embankment Dams.", *Journal of Geotechnical and Geoenvironmental Engineering* 130(4), 373–380.

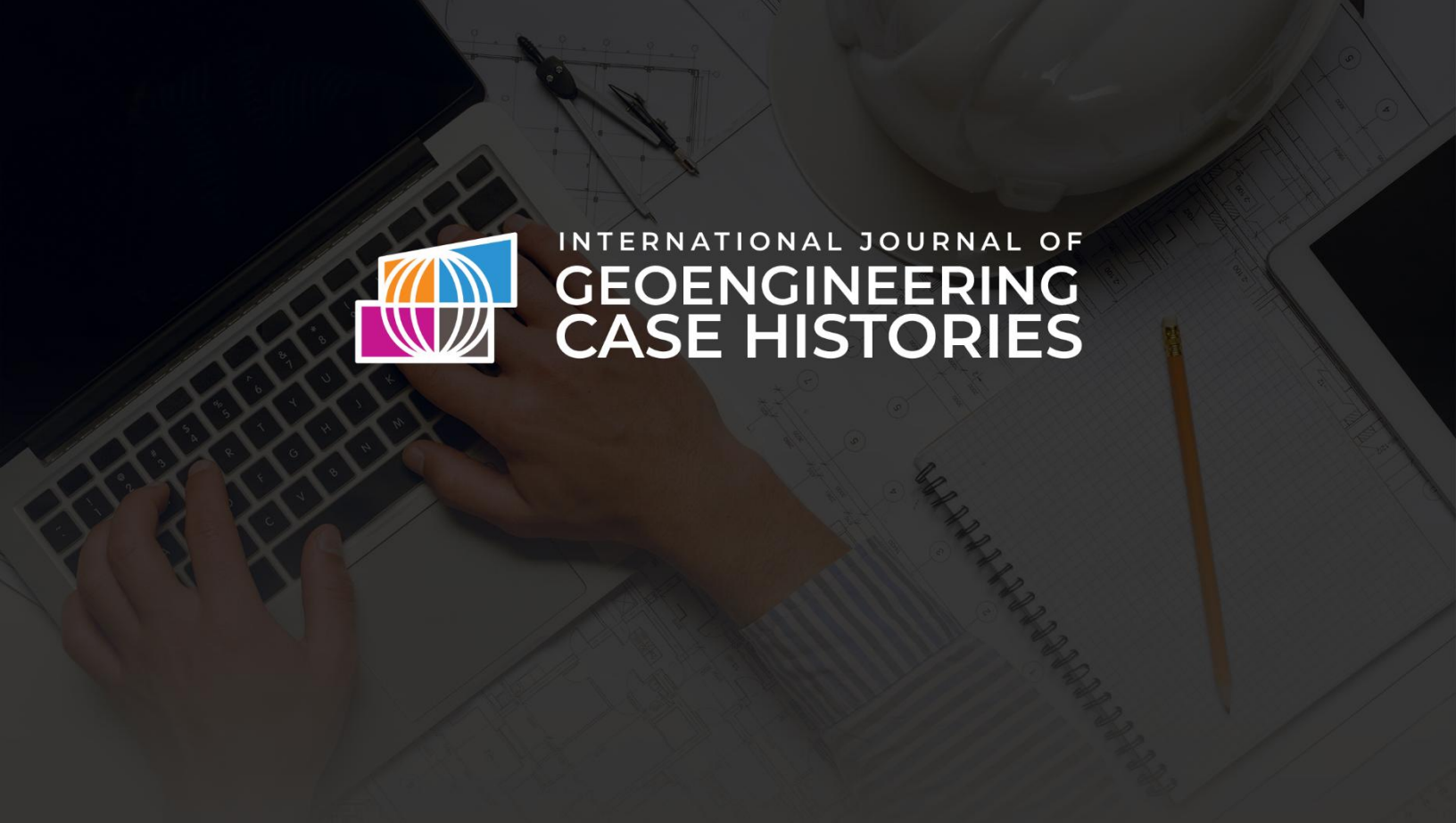

INTERNATIONAL JOURNAL OF
GEOENGINEERING
CASE HISTORIES

***The Journal's Open Access Mission is generously supported by the following Organizations:***